Deep flow variability in the vicinity of the Yucatan Straits from a high-resolution numerical simulation

Laurent M. Chérubin
Rosenstiel School of Marine and Atmospheric Science, University of Miami, Miami, Florida, USA

W. Sturges
Department of Oceanography, Florida State University, Tallahassee, Florida, USA

Eric P. Chassignet
Rosenstiel School of Marine and Atmospheric Science, University of Miami, Miami, Florida, USA

Received 14 January 2004; revised 7 July 2004; accepted 10 August 2004; published 23 April 2005.

[1] The deep flow variability in the vicinity of the Yucatan Channel between the Caribbean Sea and the Gulf of Mexico is examined within a high-resolution numerical simulation of the North Atlantic Ocean. We focus on the 6 year integral cycle of Loop Current (LC) ring formation, and we study the flow regimes both in the Yucatan Channel and farther north in the LC. The circulation in the vicinity of the Yucatan Channel presents a high variability in the flow regimes and in the shedding period, in good agreement with earlier observations. The outflow (toward the Caribbean Sea) in the Yucatan Channel is shown to be controlled in part by a regular shift of the LC maximum velocity position, in phase with the transport variations. The outflow follows the inflow variations independently of the northward extension of the LC. Our analysis of the growth of the loop is also shown to be in good agreement with the ballooning process proposed by Pichevin and Nof (1997) and Nof and Pichevin (2001) to explain the LC ring formation. Moreover, at the end of each cycle of ring formation a sudden deepening of the LC deepest layer occurs together with an intensification of the transport and of the currents in the deep layers beneath the LC. This process is shown to be connected with the growth of cyclones in the deep layers. They result from the bottom-intensified instability of the LC ring and contribute to its separation from the LC.

Citation: Chérubin, L. M., W. Sturges, and E. P. Chassignet (2005), Deep flow variability in the vicinity of the Yucatan Straits from a high-resolution numerical simulation, *J. Geophys. Res.*, *110*, C04009, doi:10.1029/2004JC002280.

1. Introduction

[2] The deep circulation associated with the generation of Loop Current rings in the Gulf of Mexico (GOM) is studied within a basin-scale high-resolution (1/12°) North Atlantic simulation using the Miami Isopycnic Coordinate Ocean Model (MICOM). In a previous simulation, the Comprehensive Ocean Atmosphere Data Sets (COADS) monthly climatological data sets [*da Silva et al.*, 1994] were used as the surface boundary conditions. *Romanou et al.* [2004] examined the results of that simulation, in which the surface circulation, with features such as the Loop Current, the Loop Current rings, their formation and shedding process, and the transport through the Straits of Yucatan and Florida, was in very good agreement with observations and with the results of previous regional numerical studies regarding the Loop Current variability in the Gulf of Mexico. In the simulation analyzed for the results presented in this paper, the accuracy of the surface boundary conditions was improved by using European Centre for Medium Range Weather Forecasts (ECMWF) daily wind forcing with the same horizontal (1/12°) resolution, incorporating extreme climatological conditions that are smoothed in the COADS climatology. Thus we may expect an even more realistic surface circulation and higher variability of the basin circulation.

[3] The Loop Current, which enters the Gulf of Mexico through the Yucatan Current and exits through the Florida Straits (where it is called the Florida Current), is a component of the Western Boundary Current (WBC) System in the North Atlantic Ocean. It occupies the eastern Gulf of Mexico and is variable in position. At one extreme, it has an almost direct path from the Yucatan Strait to the Florida Current, with a quasi-permanent clockwise recirculation known as the port-to-port regime [*Coats*, 1992; *Nowlin and McLellan*, 1967; *Cochrane*, 1972; *Hoffmann and Worley*, 1986]. At the other extreme of its position, the Loop Current intrudes into the Gulf of Mexico, forming an intense clockwise looping current as far north as 29.1°N (see Figure 1). It returns to its port-to-port configuration by slowly pinching off its extension to form a large warm

0148-0227/05/2004JC002280$09.00

core ring, which then propagates westward at speeds of 2–5 km/d [*Coats*, 1992; *Elliott*, 1982; *Shay et al.*, 1998]. *Sheinbaum et al.* [2002] estimated a net Yucatan Current transport of $23.8 \pm 1 \times 10^6$ m^3 s^{-1} for the period between September 1999 and June 2000. This is 20% less than the 30×10^6 m^3 s^{-1} accepted as a nominal transport of the Florida Current, and is also less than the 28×10^6 m^3 s^{-1} assumed for the Yucatan Current by closing the transport budget for the Antilles passages [*Johns et al.*, 2002]. This 10 month measurement could be too short for estimating an annual average, as the summer peak transport one would expect from the Florida Current observations [*Molinari et al.*, 1985; *Leaman et al.*, 1987; *Schott et al.*, 1988; *Lee et al.*, 1985; *Larsen and Sanford*, 1985] is missing.

[4] In an attempt to find a relation between the Loop Current extension and the deep flow in the Yucatan Current, *Ezer et al.* [2003] focused on the variability of the transport through the Yucatan Current. Previous attempts by *Maul et al.* [1985] to establish such a relationship were unsuccessful. However, the recent observations from the CANEK (Exchange through the Yucatan Channel) measurements by *Ochoa et al.* [2001] and *Sheinbaum et al.* [2002] explain why *Maul et al.*'s [1985] earlier observations over the sill of the Yucatan Current did not show the expected correlation of flow with the Loop Current. (The CANEK Project was initiated in December 1996 with the main objective of measuring the exchange flow between the Gulf of Mexico and the Caribbean Sea through the Yucatan Channel. 6 cruises were successfully concluded: December 1996, May 1997, March 1998, January 1999, August 1999 and June 2000. During these cruises extensive shipboard ADCP and CTD/LADCP surveys of the region have been carried out. In August 1999, an 8 mooring array, containing 33 Aanderaa current meters and eight upward looking ADCP's, was deployed across the Yucatan Channel, fully recovered in June 2000, and redeployed for final recovery on June 2001. This research was supported by CICESE, Mexico's CONACyT, and the Inter-Americas Institute for Global Change (IAI), and through contracts with Deepstar.) Specifically, these new observations show that most of the return deep flow is found along the eastern and western slopes of the Yucatan Current, and not in the middle of the sill as was previously thought. Moreover, the deep transports from the new observations are in agreement with the hypothesis set forth by *Maul et al.* [1985]: the deep outflow is correlated with the variations in the Loop Current extension. *Ezer et al.* [2003] found that the deep return transport below 800 m negatively correlates (-0.4) with changes in the Loop Current extension area, in agreement with the observational analysis of *Bunge et al.* [2002].

[5] *Welsh and Inoue* [2000], using the Modular Ocean Model with a 1/8° (14 km) horizontal grid spacing, focused on the deep layer circulation beneath the Loop Current as a ring is forming in the eastern Gulf. An anticyclone-cyclone pair, coined "modon" (horizontal dipole) in the Loop Current literature, develops beneath the Loop Current ring during the shedding event. The dipole drift contributes to the separation of the ring which then migrates westward in the surface layer. Such behavior, specifically the generation of a modon beneath the Loop Current ring, was also observed in other numerical experiments conducted by *Hurlburt and Thompson* [1982], *Indest* [1992], and *Sturges et al.* [1993]. Those experiments showed that the deep circulation in the Gulf of Mexico is characterized by an energetic eddy field. *Bunge et al.* [2002] computed the correlation between the observed transport in the Yucatan Current from the CANEK current measurements and the sea surface Loop Current extension from Advanced Very High Resolution Radiometer (AVHRR) imagery. They showed that the mode 2 along-channel deep flow in the Yucatan Current and the surface area of the Loop Current are strongly correlated. Mode 2 consists predominantly of a jet that hugs the Yucatan slope beneath the Yucatan currents, explained as a balance between the Loop Current inflow, the Florida Current outflow, the deep Yucatan Current outflow, and the Loop Current volume. However, none of the above mentioned studies established the relationship between the deep energetic events (such as an increase in current speed) and formation of deep cyclones, and the deep circulation in the Yucatan Current, nor did they identify the mechanisms involved in the formation of the deep modon. Only a few studies provide results relating to the deep circulation forcing by the Loop Current regimes in the vicinity of the Yucatan Current. *Hurlburt and Thompson* [1982] showed that barotropic instability is one of the most likely mechanisms in the shedding of eddies. A characteristic feature of this mechanism is the generation of a modon in the lower layer as the Loop Current begins to form an eddy. In the presence of sufficient deep water inflow through the Yucatan Current, the Florida Shelf topography may prevent Loop Current penetration and eddy shedding by reducing the distance between the inflow (Yucatan Current) and outflow (Florida Straits) ports; the deep water inflow and the topography thus stabilize the Loop Current. *Welsh and Inoue* [2000] proposed the *Cushman-Roisin et al.* [1990] mechanism for the generation of the deep anticyclone-cyclone pair beneath the Loop Current ring. This mechanism assumes the conservation of potential vorticity in the layer underneath the Loop Current ring as it moves on a β plane. Anticyclonic vorticity develops downstream of the eddy since the low potential vorticity layer is being squeezed; cyclonic vorticity develops upstream of the eddy as high potential vorticity water is being stretched. These conditions result in the southward advection of the eddy [*Cushman-Roisin et al.*, 1990].

[6] In this paper, after showing good agreement of the behavior of the model with the results of previous studies in the Yucatan Current, we present results pertaining to the mechanisms involved in Loop Current ring formation, as obtained in the MICOM simulations. These results are compared to those of *Hurlburt and Thompson* [1982] and the modon formation mechanism is compared to the explanation of *Cushman-Roisin et al.* [1990]. The growth of the Loop Current meander is also analyzed in light of the work of *Pichevin and Nof* [1997] and *Nof and Pichevin* [2001], regarding the ballooning of outflows. A new mechanism for the separation process, consisting of the growth of shielded vortex instability according to *Flierl* [1988], is then discussed. The paper is organized as follows: section 2 describes the model characteristics. In section 3, the variability of the transport in the Yucatan Channel over an integral number of Loop Current ring shedding events is described and compared to historical and recent results. Section 4 focuses on the Loop Current ring transport

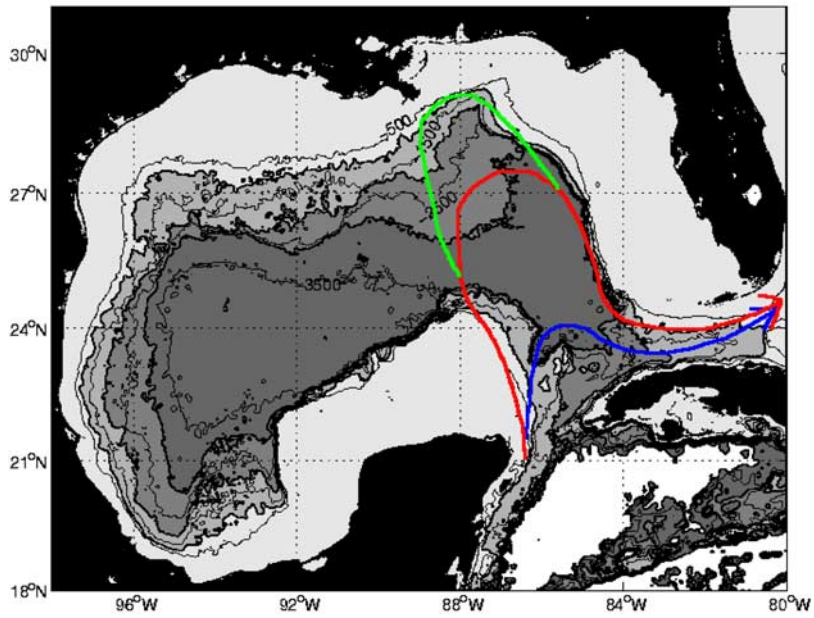

Figure 1. Mean position of the Loop Current boundary (in red) from 1980 to 1984, along with approximate maximum (in green) and minimum (in blue) penetration positions [*Schmitz*, 2001].

variability during its formation stage. In section 5 we discuss the mechanisms involved in the eddy shedding event and we compare them with the results of previous studies. Our results are summarized in the concluding section.

2. Model Description and Forcing

[7] This study builds upon previous very high resolution North Atlantic MICOM simulations that show a realistic circulation in the Gulf of Mexico [*Garraffo et al.*, 2001; *Chassignet and Garraffo*, 2001; *Romanou et al.*, 2004]. MICOM reproduces the most important characteristics of flow in the Caribbean. The total model transport through the Windward and Leeward Islands Passages into the Caribbean is 25×10^6 m^3 s^{-1}, well within the previously mentioned observational estimates of $18.4-33 \times 10^6$ m^3 s^{-1}. The mean Florida Straits transport in the model is 31.4×10^6 m^3 s^{-1}, peaking in the summer months, i.e., at the observed strength and with the correct seasonality [*Richardson et al.*, 1969; *Schott et al.*, 1988]. Model North Brazil Current rings provide most of the water for the Caribbean transport (40%), and the model reproduces the three kinds of North Brazil Current rings observed to date [*Johns et al.*, 1998, 2002; *Garraffo et al.*, 2003]. The generation rate for the rings is seven to nine per year, of which six are surface intensified, in good agreement with altimetry [*Goñi and Johns*, 2001]. The model also displays strong mesoscale variability in interisland passage transports with no clearly defined seasonality, in good agreement with what is known to date. Furthermore, the model eddy kinetic energy (EKE) in the Caribbean during the 6 year spin-up period averaged 800 cm^2 s^{-2}, ranging between 450 cm^2 s^{-2} and 1250 cm^2 s^{-2} [*Garraffo et al.*, 2001]; this agrees extremely well with a recent study by *Fratantoni et al.* [2000], whose surface drifter-based calculations showed the Caribbean EKE to range from 500 cm^2 s^{-2} to 1500 cm^2 s^{-2}. Therefore we have some confidence that this basin-scale numerical simulation with high resolution can reproduce the large-scale as well as the mesoscale variability of the Gulf of Mexico and the Caribbean Sea.

[8] The fundamental reason for modeling ocean flow in density (isopycnic) coordinates is that this system suppresses the diapycnal component of numerically caused dispersion of material and thermodynamic properties (e.g., temperature, salinity) and allows the user to prescribe/parameterize the diapycnal physical processes. This allows isopycnic models to preserve their water mass characteristics and prevents the warming of deep water masses that has been shown to occur in models framed in Cartesian coordinates [*Chassignet et al.*, 1996]. The computational domain is the North and Equatorial Atlantic Ocean basin from 28°S to 70°N, including the Caribbean Sea, the Gulf of Mexico, and the Mediterranean Sea. The horizontal grid (6 km on average) is defined on a Mercator projection with resolution given by $1/12° \times 1/12° \cos(\phi)$, where ϕ is the latitude. The bottom topography is derived from a digital terrain data set with $5'$ latitude-longitude resolution (ETOPO5). The vertical density structure is represented by 19 isopycnic layers topped by an active surface mixed layer that exchanges mass and properties with the isopycnic layers underneath. The vertical discretization was chosen to provide enhanced resolution in the upper part of the ocean. Open ocean boundaries are treated as closed, but are outfitted with 3° buffer zones in which temperature (T) and salinity (S) are linearly relaxed toward their seasonally varying climatological values [*Levitus*, 1982], with damping/relaxation time from 5 days at the wall to 30 days at the inner edge of the buffer zone. These buffer zones restore the T and S fields to climatology in order to approximately recover the vertical shear of the currents through geostrophic adjustment. After a 6 year spin-up with monthly climatological forcing, the model was integrated using surface boundary conditions based on ECMWF daily atmospheric data from 1979 to

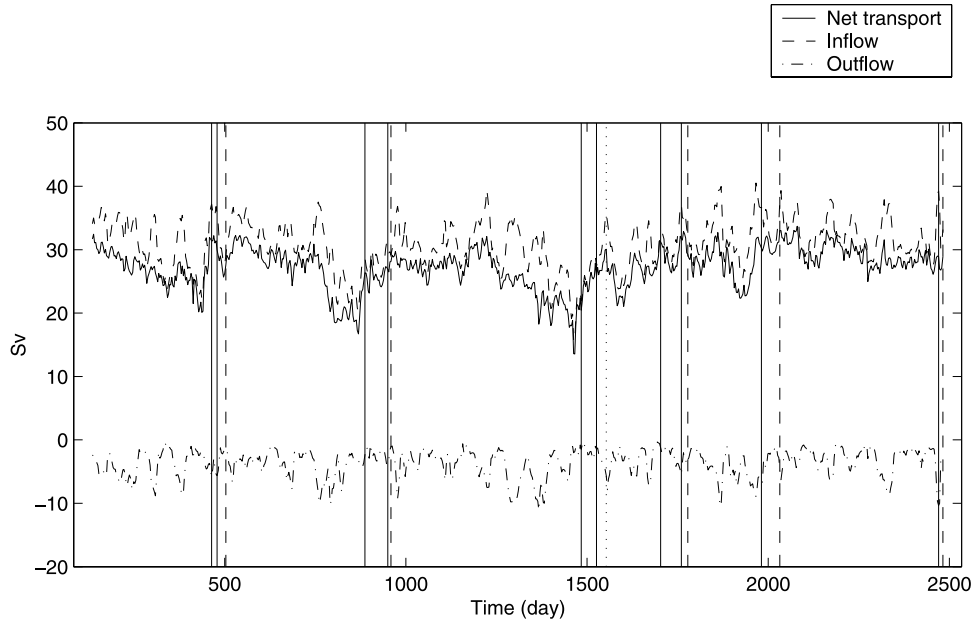

Figure 2. Time diagram over the six ring cycles of the net transport (solid line), inflow (dashed line), and outflow (dashed dotted line) in the Yucatan Current. Inflow means toward the Gulf of Mexico. The transport unit is Sverdrups.

1986. The diapycnal mixing consists of a small background value of 1 cm^2/s and a Richardson number–dependent entrainment parameterization [*Papadakis et al.*, 2003]. The high horizontal grid resolution drastically improved the model's behavior in comparison to that of previous coarse-resolution simulations. The major improvements are an excellent representation of western boundary currents (surface and deep), including a correct Gulf Stream separation [*Chassignet and Garraffo*, 2001] as well as higher eddy activity [*Paiva et al.*, 1999]. As mentioned above, the modeled Florida Straits transport is on average 31.4 $\times$ 10^6 m^3 s^{-1} (http://oceanmodeling.rsmas.miami.edu/micom), in line with observations.

3. Yucatan Straits Transport Variability

[9] *Ochoa et al.* [2001] and *Sheinbaum et al.* [2002] showed that the basic structure of the mean currents in the Yucatan Current consists of the Yucatan Current flowing into the Gulf of Mexico mainly in the western upper layers of the channel and the southerly countercurrent beneath it. However, in the upper layers, *Ochoa et al.* [2001] and *Sheinbaum et al.* [2002] observed southerly flows on both the Yucatan and Cuban coasts. Fluctuations in the currents result in significant variations in the transport through the section. *Ochoa et al.*'s [2001] and *Sheinbaum et al.*'s [2002] net transports have a mean value of 23.8 $\pm$ 1 $\times$ 10^6 m^3 s^{-1}, obtained from a 10 month current meter moorings record during the CANEK program. The transport values range from 13.5 $\times$ 10^6 m^3 s^{-1} to 31.7 $\times$ 10^6 m^3 s^{-1}. Estimating the budget of the Atlantic inflow into the Caribbean sea through the Antilles passages, *Johns et al.* [2002] obtained a 28 $\times$ 10^6 m^3 s^{-1} net transport. This value was also obtained from the difference between the Florida Straits transport (30–32 $\times$ 10^6 m^3 s^{-1}) [*Schmitz and Richardson*, 1968; *Niiler and Richardson*, 1973; *Lee et al.*, 1985; *Leaman et al.*, 1987; *Larsen*, 1992] and the Old Bahama and NW Providence Channels transport estimate of 3 $\times$ 10^6 m^3 s^{-1} [*Atkinson et al.*, 1995; *Leaman et al.*, 1995].

[10] The Loop Current mean net transport in the *Romanou et al.* [2004] COADS-forced simulation is 27 $\times$ 10^6 m^3 s^{-1}, with values ranging from 18 to 32 $\times$ 10^6 m^3 s^{-1} over a 5 year analysis, in good agreement with the results noted above. We computed 10 month versus 12 month means in the model. The average difference was only $\pm$0.3 $\times$ 10^6 m^3 s^{-1}, with the summer months removed. Therefore in the model, the seasonal variability of the Florida current is not observed in the Yucatan Current. The evolution of the Yucatan Current total transport along with the inflow and outflow to the Gulf of Mexico in our ECMWF-forced simulation, in good agreement with the above results, is shown in Figure 2 for a 7 year period. During those 7 years, six Loop Current ring shedding events occurred. Referring to the time period between two events as a cycle, each end of a cycle is marked by one ejection (shown as a solid line in Figure 2), which can be temporary (noted by two close solid lines, i.e., the first and second separation). The end of the cycle, defined by a Loop Current regime similar to that at the beginning of the cycle, is shown by a dashed line. At the end of the third cycle, the dotted line shows the shedding of a small Loop Current ring by the tip of a Loop Current intrusion. The Loop Current did not return to the port-to-port regime after this small ring shedding.

[11] Table 1 shows the mean net transport for each cycle; the average net transport in the model circulation is 27.17 $\times$ 10^6 m^3 s^{-1}. The values range between 13.5 and 33.7 $\times$ 10^6 m^3 s^{-1}, indicating stronger variations than those in the simulation of *Romanou et al.* [2004], owing to the less smoothed wind-field forcing. The first three cycles show an increase of the shedding period and a decrease in minimum net transport. By contrast, the last three cycles show a decrease of the shedding period and less variation in

Table 1. Mean Net Transport, Inflow, and Outflow in the Yucatan Current Calculated Over Each Loop Current Cycle, i.e., the Period of Formation of a Ring

	Mean Transport Over Each Cycle, Sv					
	Cycle 1	Cycle 2	Cycle 3	Cycle 4	Cycle 5	Cycle 6
Net transport	27.18	26.57	25.61	27.12	28.21	29.21
Inflow	31.12	30.25	29.76	30.15	32.42	32.32
Outflow	−3.94	−3.67	−4.09	−3.02	−4.26	−3.10

net transport. This difference in the transport trend suggests that the shedding period is not entirely dependent on the net transport in the Yucatan Current.

3.1. Flow Regimes and Dynamical Features

[12] The vertical structure of the velocity field in the Yucatan Current was, until recently, poorly described and understood. The first studies were made by *Maul et al.* [1985] based on current meter observations just above the sill at 1895 m, but because of a lack of spatial resolution of the observations, their work was unable to describe the complex flow patterns of the Yucatan Current. The observations of *Sheinbaum et al.* [2002] revealed for the first time the structure of these flow patterns, especially by finding the spatial distribution of the deep outflow from the Gulf of Mexico. A striking feature of the *Sheinbaum et al.* [2002] observations was the return flow at the surface and in the deep waters along the Cuban and Mexican sides of the Yucatan Current (see Figures 3). These shelf outflows have a strong variability, apparently related to the flow in the upper layers in the Channel.

[13] Both *Ezer et al.* [2003] and *Romanou et al.* [2004] obtained in their simulation a flow pattern very similar to the one observed by *Sheinbaum et al.* [2002]. The highest variability of the flow is at the edge of the inflow, near the Yucatan shelf, and is associated with a temporary east-west shift of the inflow core. This is an Eulerian effect, related to the meanders, and does not represent variability of the strength of the flow.

[14] Such variability and complex flow patterns are also observed in the ECMWF-forced MICOM simulations and are associated with periodic east-west shifts of the flow maximum. The upper panel in Figure 3a shows, for the six integral cycles of Figure 2, the time variation of the longitude of the velocity maximum in the first 200 m in the Yucatan Current along with the ring formations (vertical lines). The second and third panels show the longitudinal variation of the position of the western and eastern fronts defined by the outflow and inflow boundary along the Caribbean and the Mexican sides. The location of the Yucatan Current maximum oscillates longitudinally between 86.5° and 85°W with an average position at 86.1°W on the Mexican side of the channel. After each shedding event, the current maximum is shifted toward the middle of the Yucatan Current (yellow and blue stripes) and is associated with an outflow on the Mexican side of the channel (Figure 3b). The outflow occurs less frequently on the Mexican than on the Cuban side, and appears to be present on the Cuban side just before a shedding event (Figure 3c). It is, however, seen only for three of the six cycles.

[15] The longitudinal variations of the Yucatan Current maximum are correlated with the variations of the inflow transport in the Gulf of Mexico, as shown in Figure 3d. Each of the inflow peaks corresponds to an eastward shift of the Yucatan Current maximum, whereas the slowest transports correspond to a westward shift of the inflow. Similarly, the strongest deep outflows, in phase with the inflow transport variations, correspond to an eastward shift of the Yucatan Current maximum (see Figure 3e). These results show a good agreement with the *Maul et al.* [1985] conclusions, the *Bunge et al.* [2002] results, and the *Ezer et al.* [2003] simulation.

3.2. Variability Scales

[16] The Yucatan Current transport variability calculated from the ECMWF-forced MICOM simulation is now compared with the *Maul et al.* [1985] observations and the *Ezer et al.* [2003] simulation spectra. Figure 4 shows the averaged periodogram, computed with Welch's method of power spectral density [see *Welch*, 1967; *Kay*, 1987], for the net transport, the inflow, and the deep outflow across the Yucatan Current. All of the spectra show both high-frequency oscillations and long-term fluctuations that compare well with the *Maul et al.* [1985] observations and with the *Ezer et al.* [2003] model results. One of the most energetic periods, 110 days, is also obtained in the observations, but is less prominent in the *Ezer et al.* [2003] model results. *Johns et al.* [2002] obtained in their numerical model the same prominent period (110 days) associated with the transport fluctuations caused by North Brazil Current rings in the southern passages of the Lesser Antilles. In their interaction with the Lesser Antilles, the north Brazil Current rings shed some anticyclonic vorticity anomaly through the passages, which seems to promote the development of finite amplitude instabilities on the Caribbean Current. In their numerical model, *Murphy et al.* [1999] show that amplifying disturbances generated in the far eastern Caribbean by North Brazil Current rings can be traced over a period of months to the area of the Yucatan Current, where they can impact the shedding of Loop Current ring in the Gulf of Mexico. The 221 day period in the inflow and in the net transport is also very close to the 205 day period obtained both in the observations and in the *Ezer et al.* [2003] simulation. It is worth noting that the 221 day period is very likely the double harmonic of the 110 day period. In the ECMWF-forced MICOM simulation, this period is not dominant in the upper flow, but rather in the deep flows, in agreement with the *Maul et al.* [1985] results. We also have a longer-term modulation period of 507 days (17 months), which cannot be present in the 4 year model run used by *Ezer et al.* [2003]. In the deep outflow, by contrast, shorter periods dominate the spectra as in the *Maul et al.* [1985] observations.

[17] A study of Caribbean Sea eddies inferred from TOPEX/POSEIDON altimetry by *Carton and Chao* [1999] shows that these eddies are quite regular, appearing at near 3 month intervals west of the southern Lesser Antilles. Visual inspection of the TOPEX/POSEIDON record suggests that a majority of the observed eddies spin down in the western Caribbean, near the coast of Nicaragua, before passing the Yucatan peninsula. Using a 1/6° Atlantic ocean model simulation, *Carton and Chao* [1999] showed the link

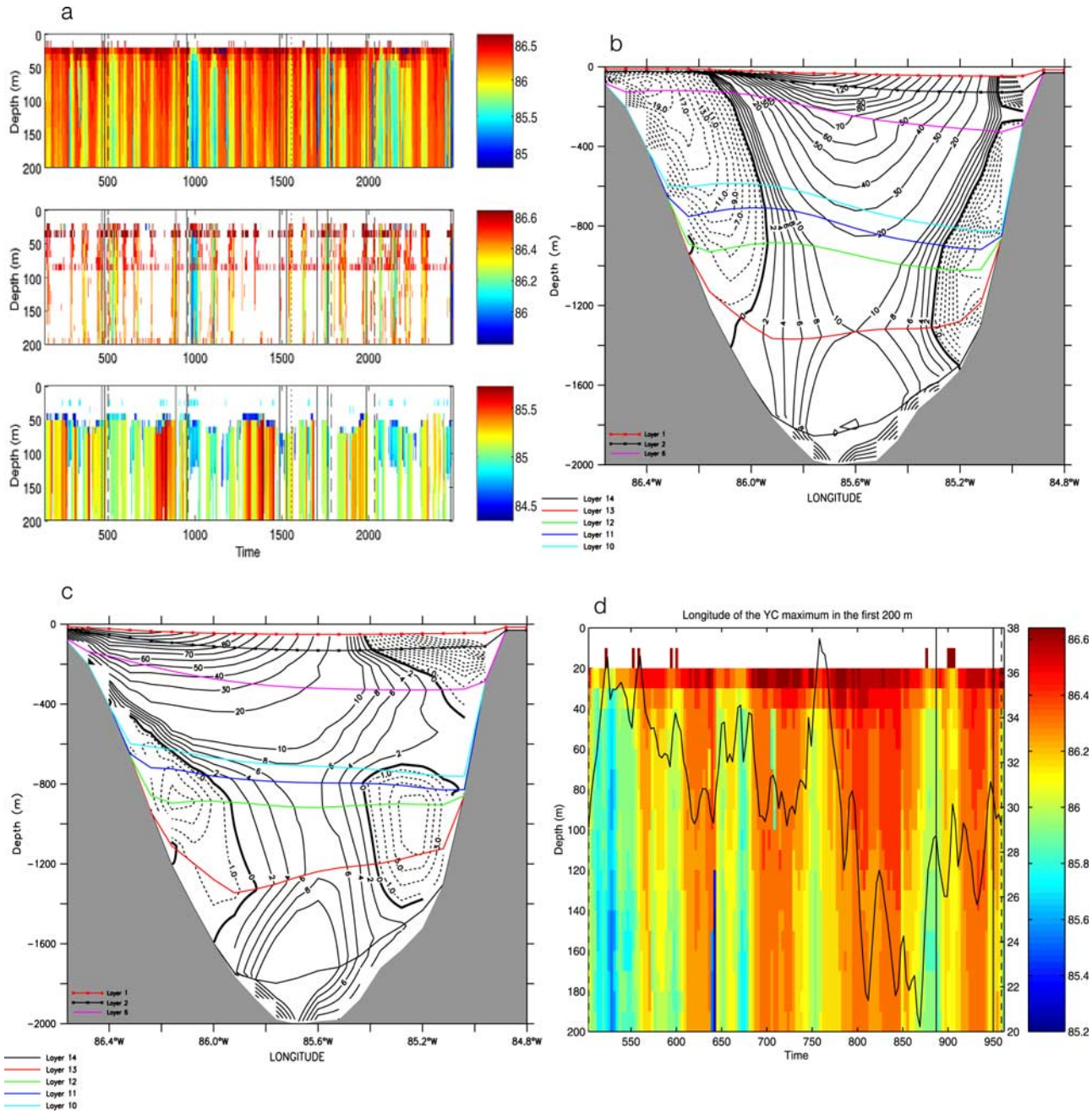

Figure 3. (a) Longitude of the velocity maximum (top), of the western front (middle), and of the eastern front (bottom) of the Loop Current in the Yucatan Current in the first 200 m depth. The color labels give the longitude in degrees. The white stripes in the middle and lower diagrams indicate that no front exists at that time. (b, c) Meridional current sections of the current through the Yucatan Current. Layer contours are displayed. The bottom layer is layer 15. These sections correspond to flow regimes in the Yucatan Current obtained during the second Loop Current ring cycle shown in Figures 3d and 3e: Figure 3b, day 540; Figure 3c, day 840. (d) Same as the upper diagram of Figure 3a for the second cycle. The solid line shows net transport in the Yucatan Current. (e) Same as Figure 3d, with the deep outflow in the Yucatan Current superimposed (dashed line).

between North Brazil Current rings impinging on the Lesser Antilles and the formation of the Caribbean eddies. Most of the simulated variability in the 50–100 day band is also the result of westward eddy propagation.

[18] As part of the Caribbean Sea eddies, Hispaniola eddies spun up by the wind stress curl are studied by *Oey et al.* [2003]. Here, both the eddies spun up by the wind and those that originate from the North Brazil Current rings are called Caribbean Sea eddies. In their numerical simulation of the Intra-Americas Sea, *Oey et al.* [2003] showed the formation of warm lenses southwest of Hispaniola. The eddies grow to a diameter of ≈300 km and drift westward,

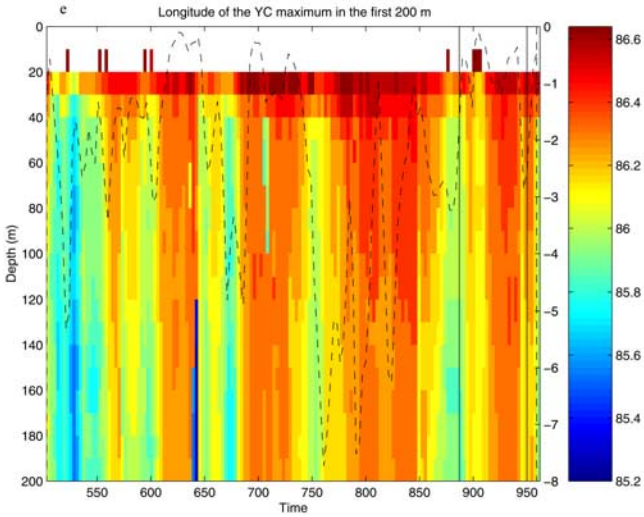

Figure 3. (continued)

following the same path as the Caribbean eddies that originate from the North Brazil Current rings. Analysis of the entire model record indicates that the cycle of eddy formation and drifting repeats at periods of 60–130 days. *Oey et al.* [2003] noticed that these periods densely cluster around a mean of 103 days. This simulated period agrees well with the estimates from our simulation.

[19] In summary, the ECMWF-forced MICOM simulation shows a surface flow whose mesoscale variability (65–110 days) also appears to depend on the Caribbean eddies' impact in the Yucatan Current, while deep flow fluctuations are made up of higher-frequency events as observed by *Maul et al.* [1985]. Most of the discrepancy in the relative power of the spectra peaks is likely to result from the difference between the measurement and simulation durations, since the same periods are qualitatively obtained.

4. Flow Regimes in the Loop Current During the Rings Formation

[20] We now focus on the Loop Current transport during the formation of the rings. To do so, we estimate the transport through a meridional section (84.8°W) between the Florida shelf and the western tip of Cuba. This section was chosen to estimate (1) the transport feeding the Florida Current and (2) the transport back to the Loop Current eddy. Comparing the previous transports with the transport in the Yucatan Current, the part of the outflow in the Yucatan Current forced by the Loop Current eddy can also be estimated.

[21] The total transport into the Gulf of Mexico via the Yucatan Current is basically balanced by the transport between Florida and Cuba, for there can be very little storage of water. Our findings here are that the dynamical features of the surface transport are very similar to those from *Ezer et al.*'s [2003] model; this did not necessarily have to be true, because of the variety of possible deep flow configurations in the Yucatan Channel. During the ring formation, an increasing part of the transport in the Loop Current, toward the Florida Current, returns westward to the Loop Current (see Figure 5).

[22] Figure 5 presents the net, the eastward, and the westward transports through the meridional section at 84.8°W, between Cuba and the Florida Straits, against time, over the 6 integral cycles of Loop Current ring formation as defined in Figure 2. The Loop Current net transport shows the same fluctuations as in the Yucatan Current, influenced by the shedding events. Disregarding of cycles 4 and 6, the net transport decreases before separation and suddenly rises at the shedding event. This sudden rise is the most characteristic event, and it is also observed in the *Ezer et al.* [2003, Figure 8b] results. The main difference between the two model results is that *Ezer et al.*'s [2003] model net transport in the Yucatan Current always decreases abruptly after the separation, while the net transport in the MICOM simulation remains as high as during the separation process (for example, in the second and third cycle). However, in the Loop Current eddy, the variations of the eastward and westward transports are more sensitive to the shedding events than in the Yucatan Current. Each separation is preceded by, or is simultaneous with, an increase in current speed in both directions. The symmetric increase in the eastward and westward directions suggests a spinning of the flow in the Loop Current ring before the separation.

4.1. Deep Water Circulation

[23] The conservation of transport between the Yucatan Current and the Florida Straits is achieved in the model primarily between the surface and 800 m (i.e the bottom of layer 11 or σ_θ = 27.52; see Table 2. The deep water transports across 84.8°W (see Figure 5b) are therefore calculated below layer 11 and are shown in Figures 6a and 6b. These two figures indicate that 50% of the transport increase during one ring formation cycle occurs in the deep layers, entailing an increase in the depth of layer 12 in the Loop Current meander, as the azimuthal speed increases in this layer (see Figure 6c). The water between 800 m and the bottom of layer 12 is entrained by the upper vortex, which increases the speed of the flow as well as its depth. This water recirculates underneath the Loop Current ring. The depth of the bottom interface of layer 12 reaches a maximum followed by the eddy separation. Afterward, layer 12 becomes shallower and thinner by about 200 m, until the Loop Current meander is replenished before the next separation. The correlation coefficient between the Yucatan Current transport and the maximum depth of layer 12 over the six cycles is 0.427. This value shows that the transport in the Yucatan Current is not the only factor controlling the period of formation of the Loop Current rings. One can speculate from the sudden transport increase that this event is related to an unstable process that grows when necessary conditions are satisfied. Those conditions would depend on the stage of the growth of the Loop Current meander. Moreover, the deep outflow in the Yucatan Current is weakly correlated to the westward flow in the Loop Current (0.289), implying that the deep outflow in the Yucatan Current is weakly controlled by the Loop Current growth.

[24] The spectral analysis is now performed on the zonal transports in the Loop Current eddy and compared with the one of the transports in the Yucatan Current. The spectral density peaks in the Loop Current total transport at 84.8°W are the same as for the inflow in the Yucatan Channel but

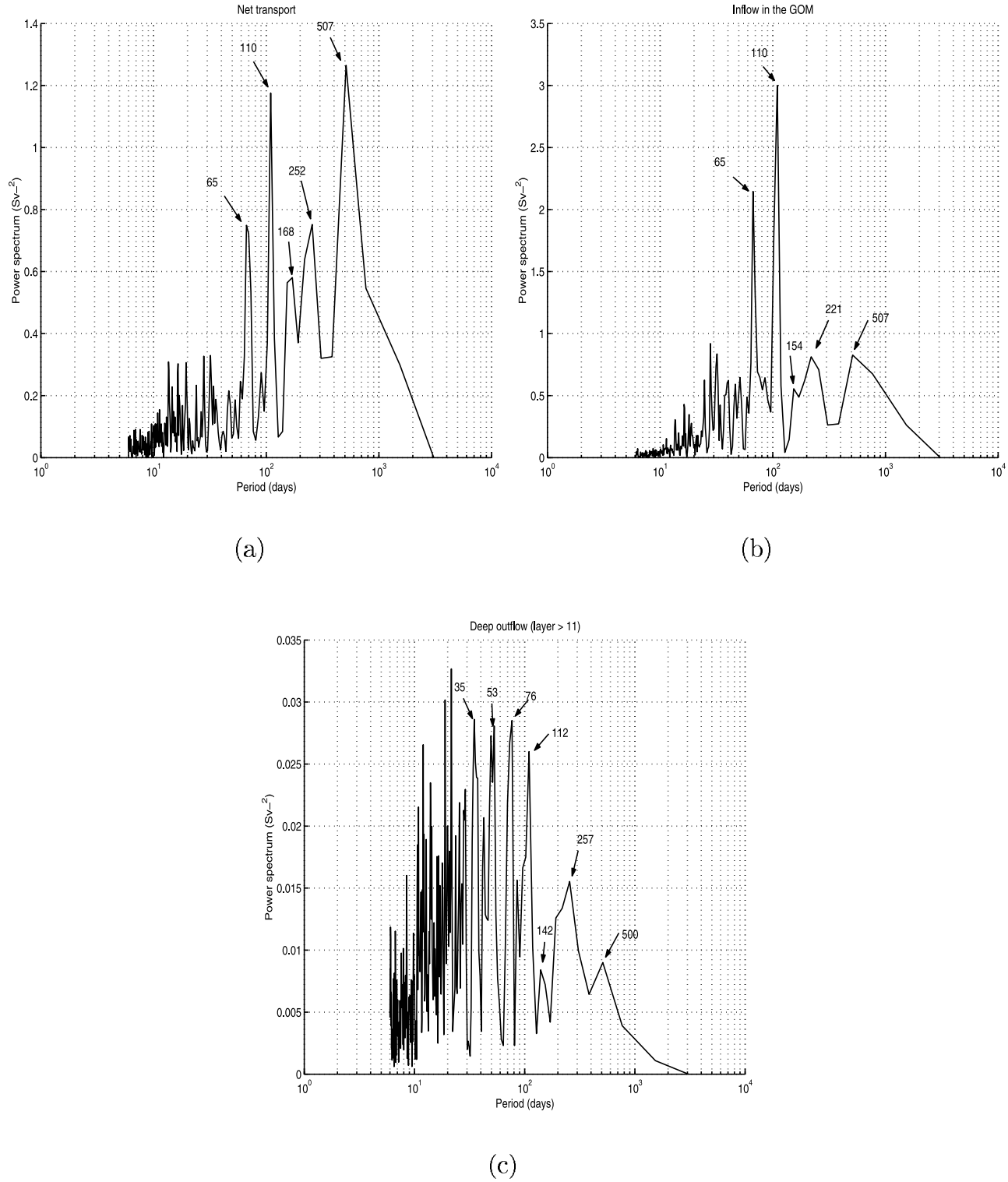

Figure 4. Power spectra (a) of the net transport, (b) of the inflow in the Gulf of Mexico, and (c) of the deep outflow, below layer 11 of the model, in the Yucatan Current.

with more short-term and long-term fluctuations (not shown), and with prominent 252 (8.4 month) and 507 day peaks. The zonal transport shows a dominant 221 day period as in the *Maul et al.* [1985] observations, with other peaks of less than 100 days (see Figure 7a). In the deep westward flow, the 8.4 month period becomes dominant in the long-term fluctuations (Figure 7b), while in the spectra of the depth of layer 12, the 221 day and 17 month peaks dominate (not shown). The 8.4 month period appears as characteristic of the ring formation process because it is associated with the deep spinning flow increase in the Loop Current ring, which is controlled by the shedding process.

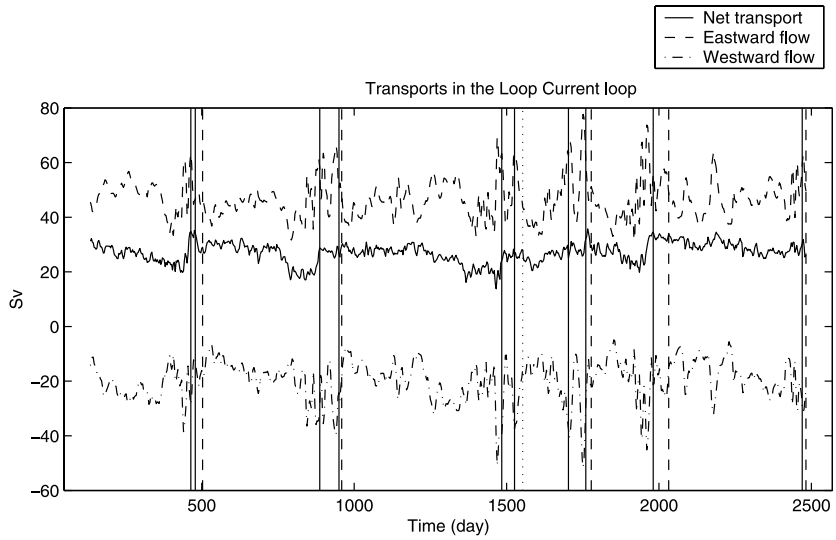

(a)

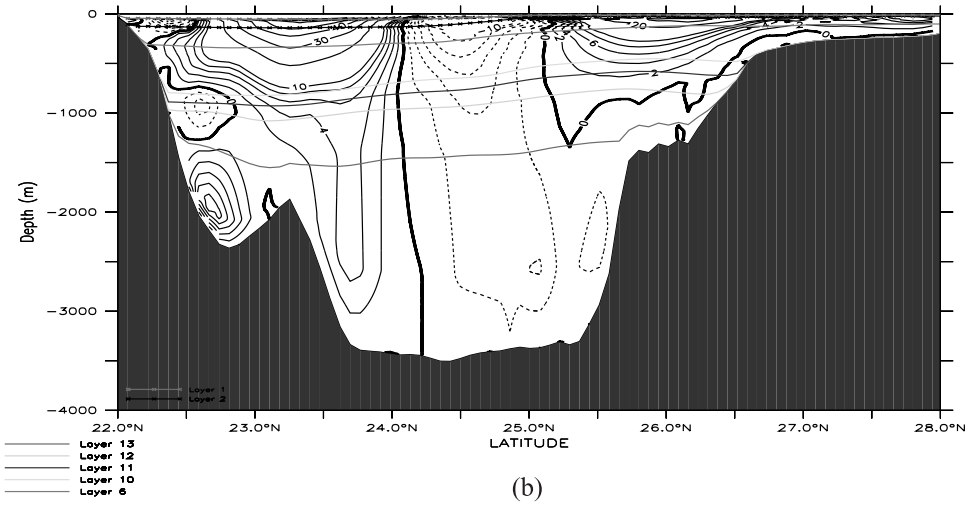

(b)

Figure 5. (a) Same as Figure 2 for the Loop Current in the Gulf of Mexico across a meridional section at 84.8°W between Cuba and the Florida shelf. (b) Mean zonal current section at 84.8°W across the Loop Current ring over the first cycle.

This period is very close to most of the shedding intervals observed by *Maul et al.* [1985], *Sturges* [1992], *Sturges et al.* [1993], and *Vukovich* [1995].

4.2. Ballooning Mechanism

[25] The growth of the Loop Current meander, as observed in the MICOM simulation, exhibits the characteristics of a growing bulge at a cape with a downstream coast on the right of the current (Cuba). *Pichevin and Nof* [1997] and *Nof and Pichevin* [2001] addressed the unsteady behavior of such an anomalous density current emptying into an open basin at a cape. They showed that, due to the impossibility of balancing the alongshore momentum flux, the outflow balloons near its source, forming an anticyclonic bulge. They proposed this mechanism as an explanation of why the Loop Current always loops in the same general area. The *Pichevin and Nof* [1997] mechanism of formation can be divided into two steps. First is the ballooning of the current, where in the case of intense outflows (strong relative vorticity O(−f)) associated with a rapidly growing bulge, 66% of the outflow mass flux goes into the bulge and the remaining 33% goes into the downstream current. The second step is the separation of the ring by the β and/or topographic effect [see also *Hurlburt and Thompson*, 1980], when 80% of the inflow goes into the downstream current and 20% into the eddy. *Nof and Pichevin* [2001] applied their results to the Loop Current. Assuming a 30×10^6 m^3 s^{-1} flow transport, 300 km ring radius and 1000 m vortex thickness, they obtained a 300 day generation periodicity. The separation of the bulge is driven by the β effect, which in their scenario takes 200 days to force it to detach. The eddy generation period, however decreases against the flow transport. Their results are therefore consistent with both observations and models.

Table 2. Density Anomaly of the 20 Layers of MICOM

Layer	σ_θ
1	mixed layer
2	24.70
3	25.28
4	25.77
5	26.18
6	26.52
7	26.80
8	27.03
9	27.22
10	27.38
11	27.52
12	27.64
13	27.74
14	27.82
15	27.88
16	27.92
17	28.00
18	28.06
19	28.09
20	28.12

[26] In our numerical simulation, we computed the ratio (in relation to the total inflow) of the return flow to the Loop Current bulge and obtained a fair agreement with the assessment of *Pichevin and Nof*'s [1997] theory. Figure 8 shows that during the ballooning, the return flow to the loop is, on average, 40% of the total inflow, with a maximum of 60%. Just before the separation this percentage drops to 20%. These results are therefore consistent with the momentum imbalance paradox as a mechanism of formation of the Loop Current rings.

5. Discussion

[27] The analysis of the modeled Loop Current flow regimes in the previous section suggests that several mechanisms may be at work in the ring formation and separation process. Mechanisms that have been shown to be self sufficient to shed a Loop Current eddy are described as follows: (1) In their numerical simulations, *Pichevin and Nof* [1997] and *Nof and Pichevin* [2001] showed that in the ballooning mechanism, described in the previous section, the bulge separates from the current after a growing phase and no instability is involved in the separation process. The separation is achieved by the westward advection of the newly formed eddy due to the β effect on the bulge for a determined size. (2) *Sturges et al.* [1993] and *Welsh and Inoue* [2000] examined the deep current circulation during the generation and, more specifically, during the westward propagation of the Loop Current ring in their numerical models. They observed the generation of cyclonic and anticyclonic circulations underneath the ring in formation, and *Cushman-Roisin et al.* [1990] proposed a mechanism involved in the generation of the deep dipole, described in the introduction. (3) In *Hurlburt and Thompson*'s [1980] two layer simulation, barotropic instability plays an important role in the formation of an anticyclone-cyclone pair, or modon, in the lower layers. During the westward migration of the ring, the orientation of the axis of the modon is close to the direction of propagation of the ring, with the anticyclone leading. In *Cushman-Roisin et al.*'s [1990] explanation, it is in fact the motion of the anticyclone that generates the modon, and not an unstable process.

[28] In this section, we suggest that a combination of the above mechanisms is involved in the Loop Current ring formation process. Such a combination of processes was analyzed by *Serra et al.* [2002], who studied experimentally the formation of dipolar structures at a cape by an upstream current. Their results were in good agreement with observations. They proved that the Rossby and Froude numbers of the current upstream of the cape are the determining factors in predicting the behavior at the cape. For sufficiently low Rossby number ($0.1 \leq Ro \leq 0.6$), the laboratory measurements show that there is formation of a dipolar structure at the cape, either by instability of the current at the cape or by coupling of an anticyclone created at the cape by the current (growing bulge) and of a cyclone created upstream and advected by the current. In our simulation, the Loop Current ring formation exhibits the combination of the growth of a bulge, as explained by the ballooning mecha-

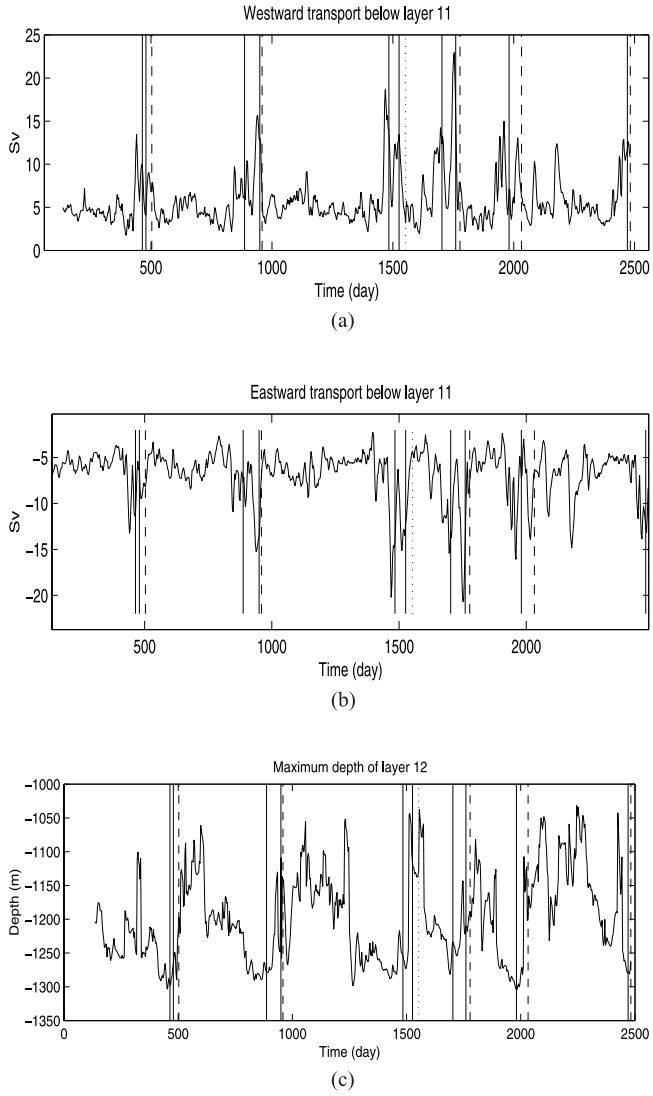

Figure 6. Deep (below layer 11 of the model) (a) westward and (b) eastward transport in the Loop Current across the meridional section described in Figure 5 and over the six eddy cycles. (c) Maximum depth of layer 12 underneath the Loop Current loop center.

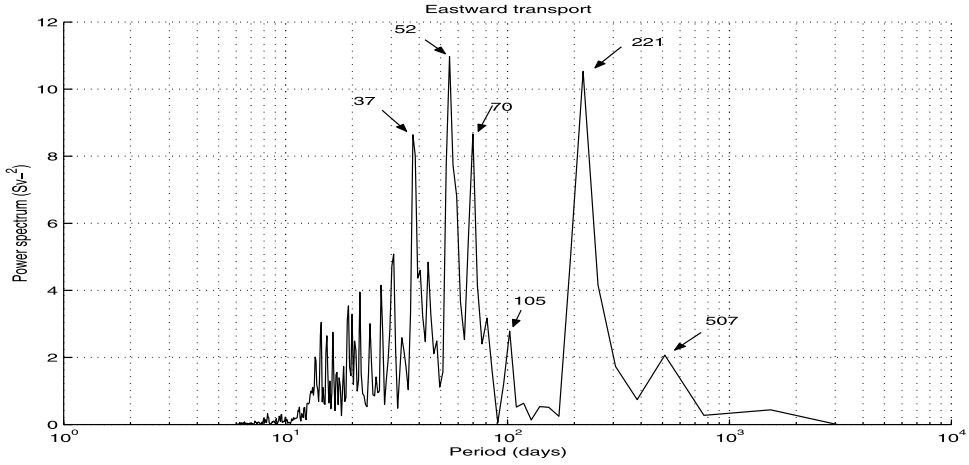

(a)

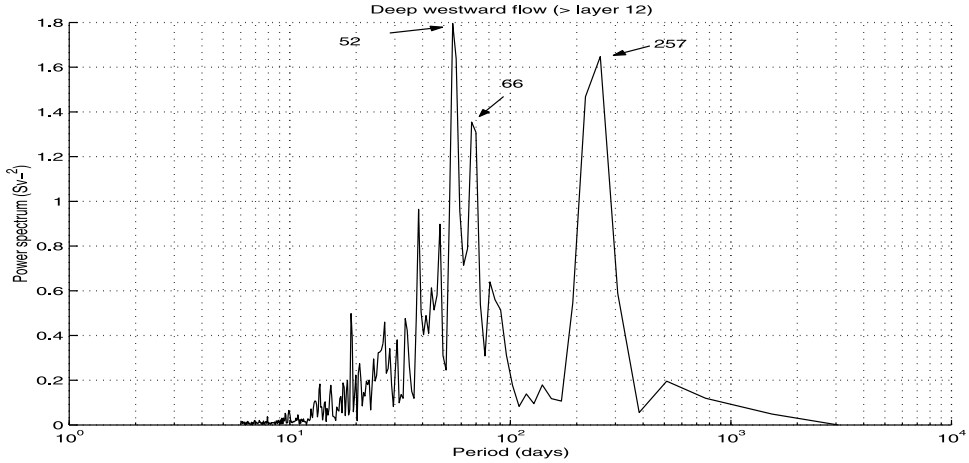

(b)

Figure 7. Power spectra of the (a) eastward and (b) deep westward transport in the Loop Current.

nism, and an unstable process, which is the sudden and rapid deepening of the active layer (Figure 9a) underneath the Loop Current ring and the spinning of that layer (Figure 9b). Furthermore, three cyclones are generated at the rim of the deep part of the anticyclone (see Figure 10). In order to show that the cyclones generation is the product of an instability, we compute from the model outputs the amplitude of the first four azimuthal modes during the stage of formation of the Loop Current ring until the early formed eddy begins to drift westward. We focus here on the first cycle since the ring formation in the other cycles is very similar.

5.1. Vortex Instability

[29] As the modal analysis depends on the efficacy of the modal decomposition, our algorithm was validated by application to a reference case for which the most unstable growing modes are known. The reference case consists of an unstable vortex whose most unstable mode is $m = 4$. The nonlinear steady state is axisymmetric, with four cyclones

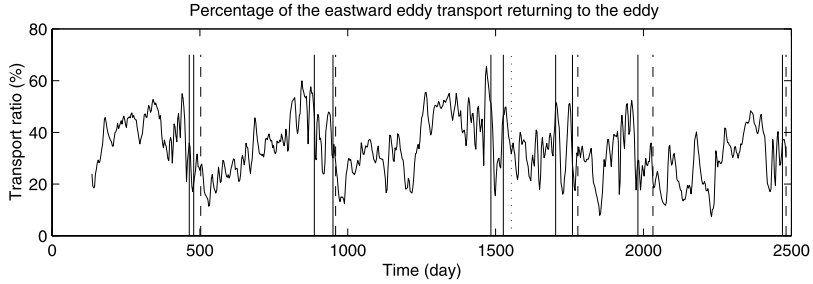

Figure 8. Percentage of the incoming transport returning in the loop over the six eddy cycles.

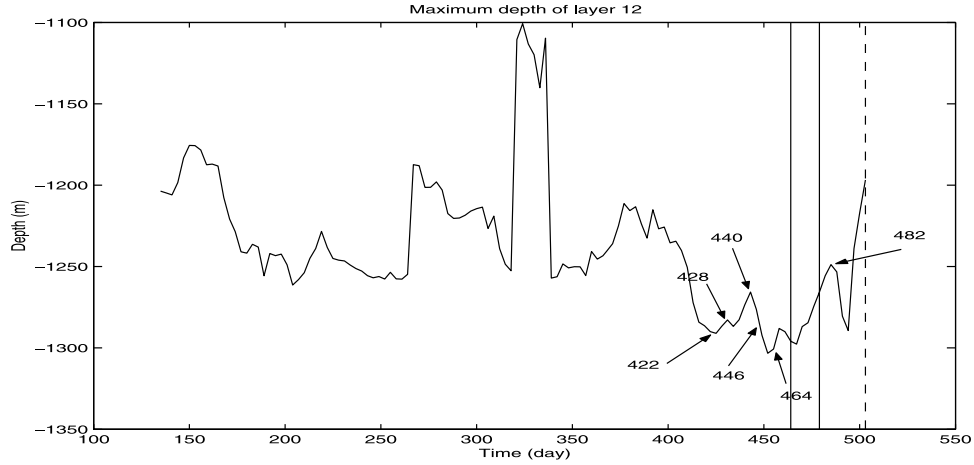

(a)

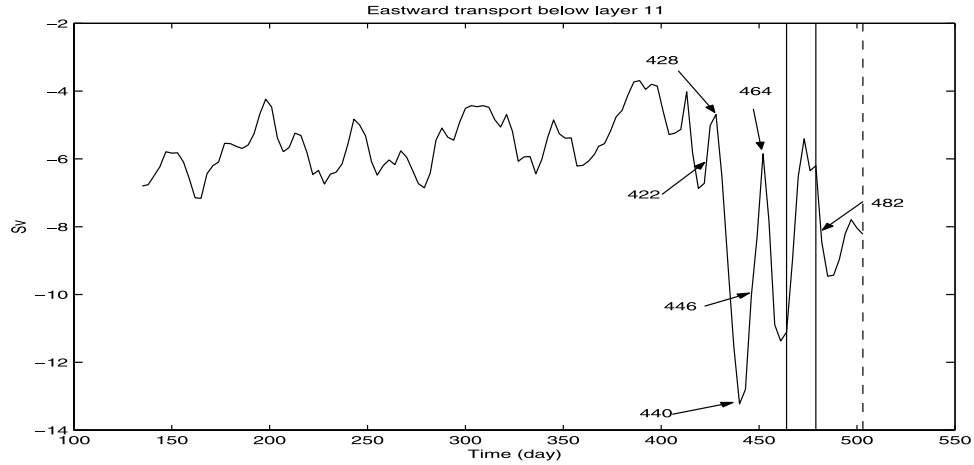

(b)

Figure 9. (a) Maximum depth of model layer 12 during the first cycle. (b) Deep eastward transport in the Loop Current during the first cycle. The numbers are days and correspond to the frames displayed in Figure 10.

surrounding an anticyclone, the whole structure thus forming a pentapole. The modal decomposition was successfully applied to the evolution of the vortex both on an f plane and on a β plane as shown by Figures 11a and 11b respectively. On the f plane, mode 4 is the dominant and fastest growing mode (Figure 11a). On the β plane, mode 1 is the fastest growing mode. The other modes overtake after some delay and mode 4 is not then dominant (Figure 11b). The general method used in this modal decomposition is now described. We first calculate the nonaxisymmetric part of the vortex:

$$\delta h(r,t) = h_T(r,t) - \bar{h}(r,t), \tag{1}$$

with h_T the local layer thickness and $\bar{h}(r)$ the axisymmetric part of the layer thickness:

$$\bar{h}(r,t) = \frac{1}{2\pi}\int_0^{2\pi} h(r,\theta,t)d\theta. \tag{2}$$

Then for a particular azimuthal mode m, the modal components are defined as

$$\{C_m(r,t), S_m(r,t)\} = \frac{1}{\pi}\int_0^{2\pi} \delta h(r,\theta,t)\{\cos m\theta, \sin m\theta\}d\theta, \tag{3}$$

with the amplitude

$$\bar{A_m}(r,t) = \frac{1}{r_{\max}}\int_0^{r\max} \left[C_m^2(r,t) + S_m^2(r,t)\right]^{1/2} dr, \tag{4}$$

where $r_{\max}$ is a characteristic radius of the perturbed vortex. The mode amplitudes (m = 1, 2, 3, 4) are presented in Figure 11 for deep Loop Current ring layer 8 (σ_θ = 27.38; see Table 2) and surface layer 1, which is the mixed layer. To help the reader visualize the modes, their spatial structure in terms of height above or below the mean layer thickness is shown in Figure 12.

[30] In the chronology of the transport events, the maximum depth occurred at day 446, as shown in Figure 9a.

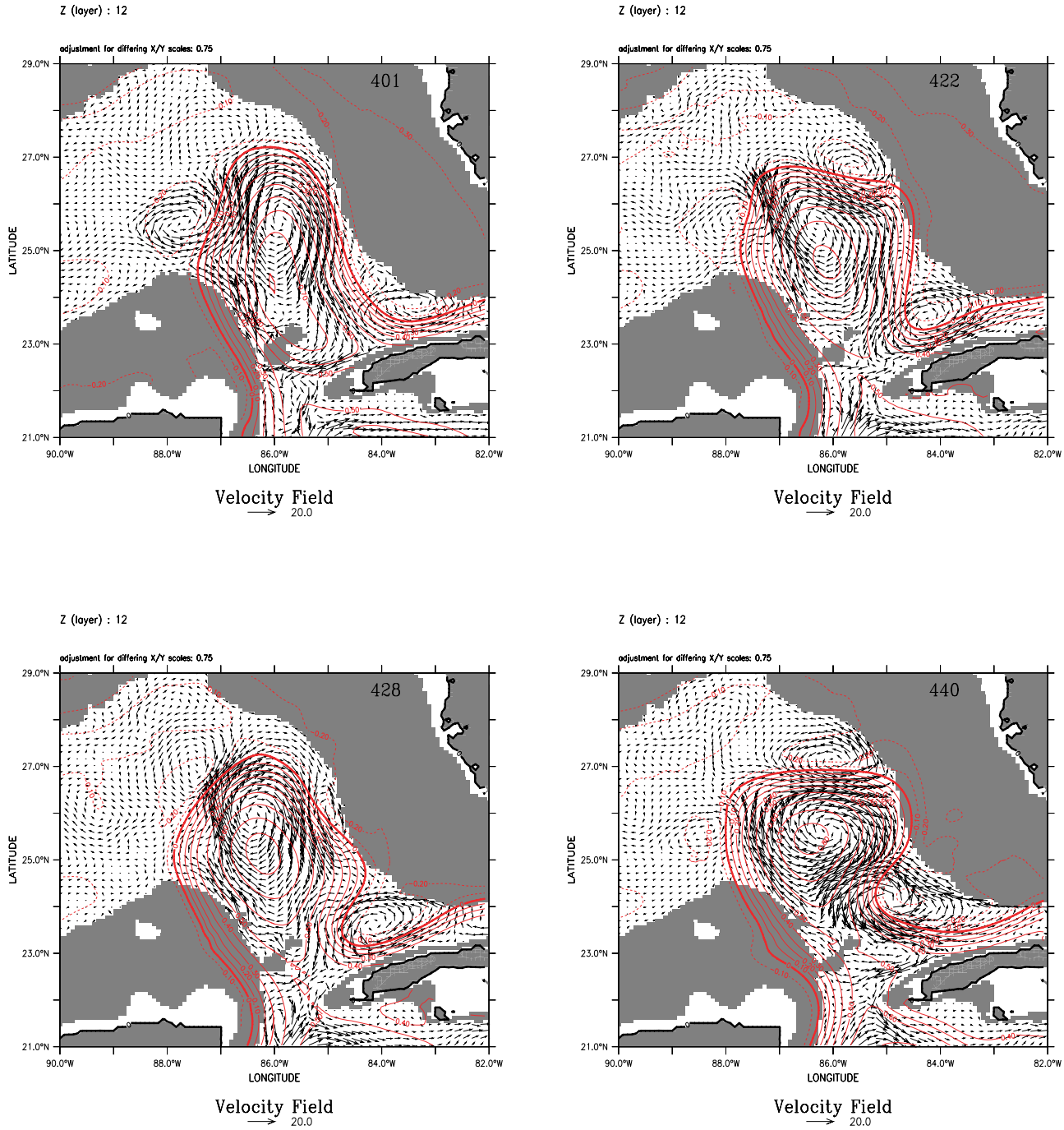

Figure 10. (a–l) Frame sequence of the flow circulation in layer 12 superimposed on the sea surface height (red contours in meters). Solid lines are positive contours. The shading corresponds to the bottom topography mask. The number in the caption is the day. The scale (cm/s) of the arrows is given by the vector length just below the frame. (m) Stick diagram of current obtained in MICOM simulation at the same location (25°36.2′N and 85°29.8′W) as *Hamilton*'s [1990] mooring G during the same Loop Current cycle. From top to bottom, three depths are displayed: 2500, 1500, and 400 m.

Figures 11c and 11d show an increase of the mode amplitudes around day 446 in layers 1 and 8. In both layers, the distribution of the mode amplitudes is the same as for those of a pentapole on a β plane (Figure 11b), i.e., mode 1 dominates mode 2, which dominates mode 3, which dominates mode 4. Most of the spatial variance is explained by the first mode during the growing phase, as shown by Figure 11e. Therefore the final product of this instability would be a horizontal dipole as obtained in the reference case on the β plane (Figure 11f). Indeed, the β effect induces the growth of mode 1 [*Sutyrin and Flierl*, 1994; *Sutyrin and Morel*, 1997], while the growth of mode 2 (called the

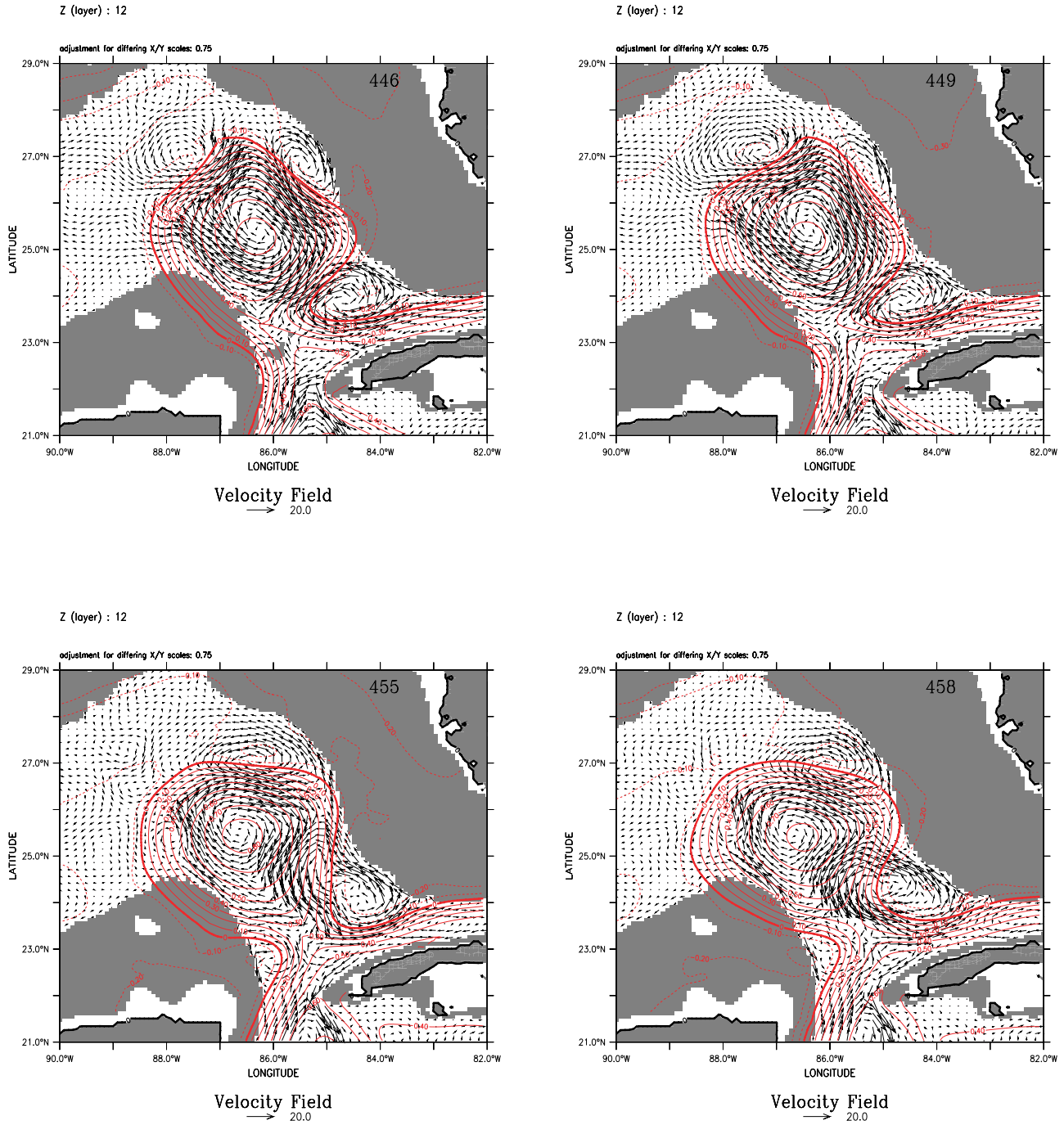

Figure 10. (continued)

elliptical mode) is related to the vortex displacement [*Sutyrin and Flierl*, 1994; *Sutyrin and Morel*, 1997]. This result suggests that the event occurring in the Loop Current ring in the ECMWF daily forced MICOM simulation is the growth of a vortex rim instability.

[31] The product of the nonlinear growth of modes 3 and 4 in the (Loop Current ring) instability, both in the deep layers and at the surface, is the formation of three or four cyclones that will propagate around the eddy rim (Figures 10e and 10f), probably strongly constrained by the topography of the Campeche Bank, Florida shelf, and Cuba coast. Since this instability does not break up the eddy, one or two cyclones survive between Cuba and the Florida shelf if they are not damped by friction or topographic effects. This mode 3 or 4 instability can explain the peculiar shape (triangular) of the Loop Current rings when they separate from the Yucatan Current, as shown by Figure 10k and by many ring contours drawn from AVHRR images [see *Fratantoni et al.*, 1998]. As mode 4 is the fastest growing mode at the beginning of the instability (Figures 11c and 11d), one can assume that the steady nonlinear state of an isolated Loop Current ring is a pentapole.

[32] In the frames of Figure 10, one can also see the vertical tilt of the vortex as a result of the instability [*Flierl*,

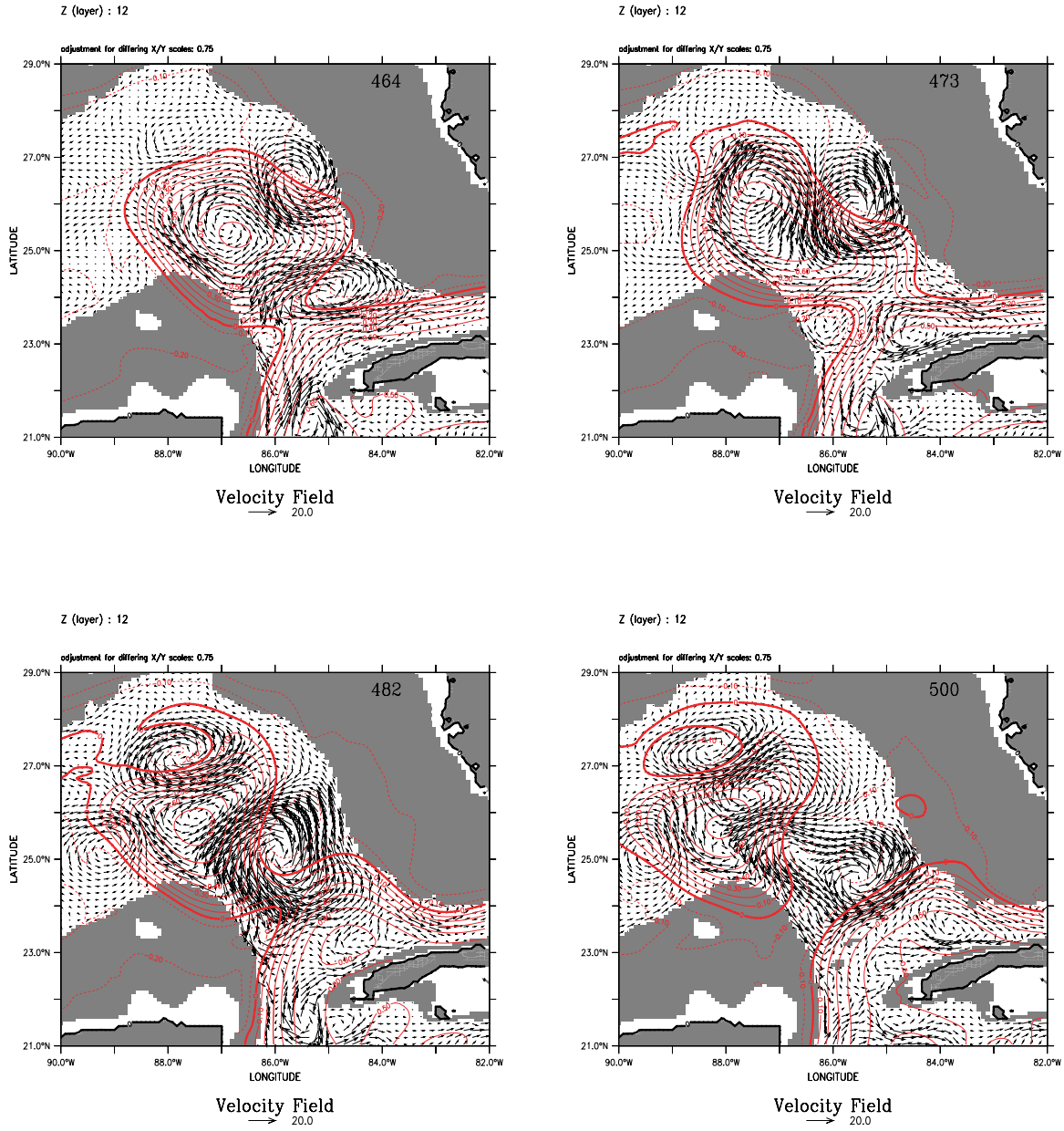

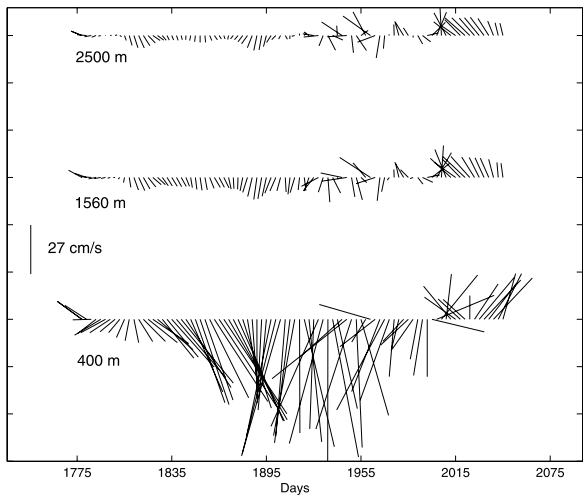

Figure 10. (continued)

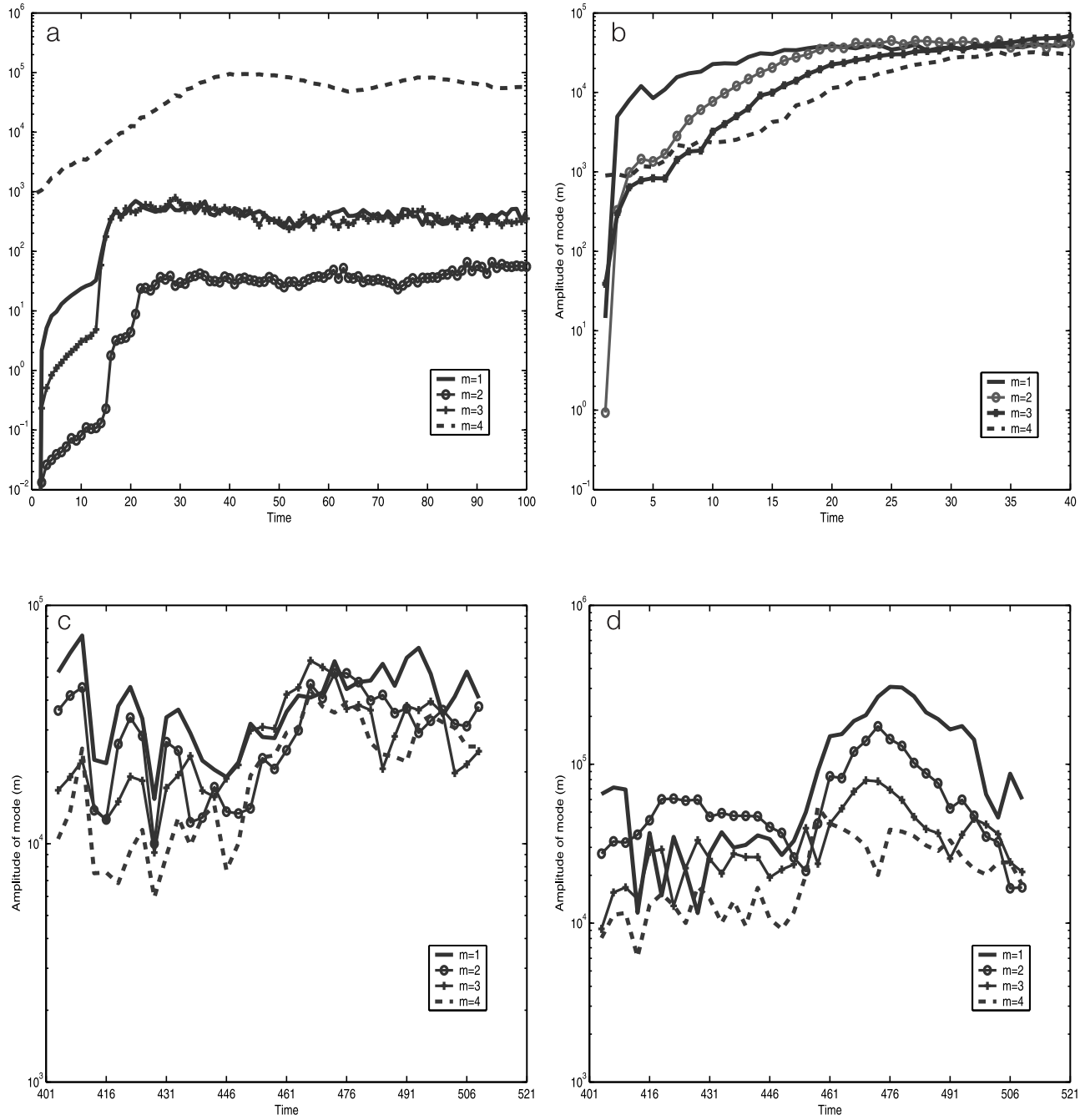

Figure 11. (a) Instability of a shielded vortex on a *f* plane: time variation of the amplitude of modes 1, 2, 3, and 4 for a reference case where mode 4 is the most unstable. The vortex restabilizes as a pentapole (four cyclones). (b) Same vortex on a β plane. (c) Time variation of the perturbation amplitudes in layer 8 for the same modes as in the reference case in the MICOM simulation during the first Loop Current ring cycle. (d) Same as Figure 11c in the surface layer. (e) Percent of spatial variance explained by each of the modes. (f) Tripole as a degenerate pentapole on a β plane. Dashed and shaded contours show cyclones, while solid lines contour the anticyclone.

1988]. The vortex deep layer signature of the cyclones reveals the generation of barotropic motion around the vortex. The vertical tilt and barotropic motions appear as being the product of the instability of geostrophic vortices as presented by *Flierl* [1988]. In particular, barotropic isolated vortices, such as a circular region of horizontally uniform potential vorticity surrounded by an annulus of uniform (but different) potential vorticity, are unstable when the outer annulus is sufficiently narrow, e.g., when the ratio between the interior and exterior radii is close to 1. *Flierl* [1988] shows that the higher modes ($\geq$3) can grow faster than the lower modes for a given range of external radii. When the isolated vortex is submitted to baroclinic perturbations, twisting and tilting may also

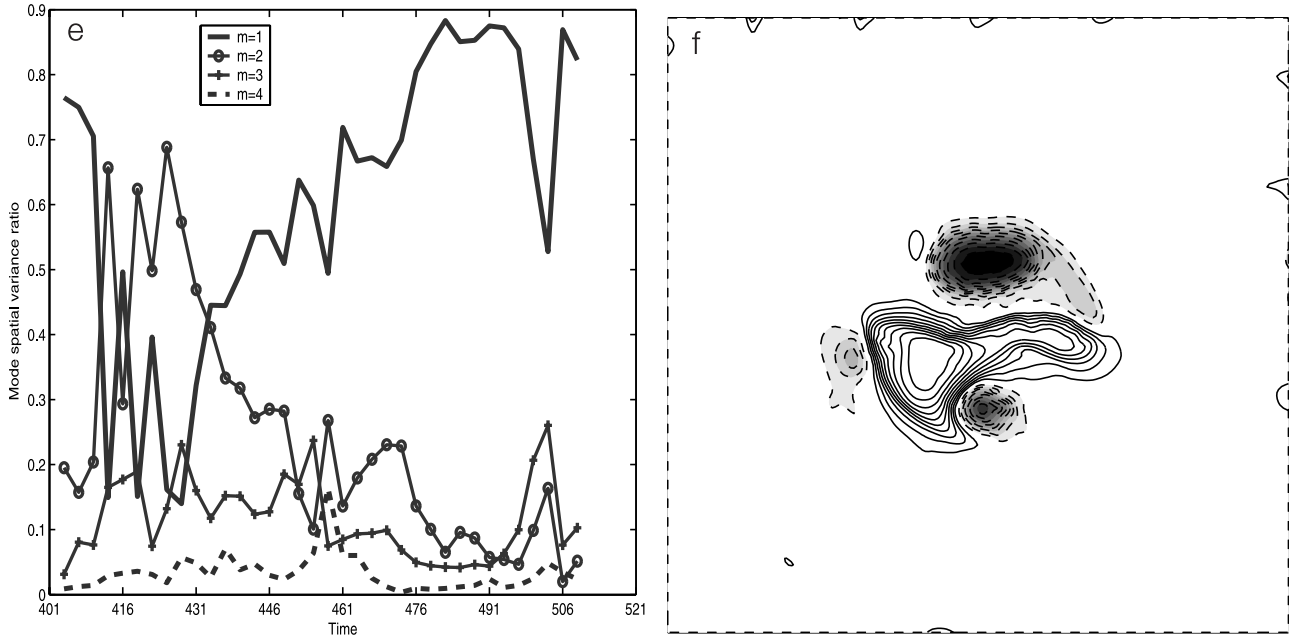

Figure 11. (continued)

develop with the growing instability. However, *Flierl* [1988] does not show whether such vortices, with a narrow and strong outer shear zone, have a supercritical (equilibrating) mode 3 or 4 instability. Nevertheless, this mechanism would explain why the spinning due to the growth of the cyclones (see the difference between Figures 10c and 10d) in the deep layer is so sudden, and why the vortex does not break up if the instability would become supercritical. Moreover, *Candela et al.* [2002], from observations in the Yucatan Current, show the strong positive PV anomaly on the western side of the Yucatan Current, which generates an outer sheared belt around the Loop Current. This is also observed in our MICOM simulations.

[33] It is worth noting that this deepening scenario is observed in *Hamilton*'s [1990] data, on his mooring G located at 25°36.2′N and 85°29.8′W in the eastern Gulf of Mexico on the western Florida shelf. The eddy formation first occurs in the same month of the same year (i.e., the year of the wind forcing) as in the numerical simulation. It corresponds to the fifth Loop Current ring cycle in Figure 5a. In *Hamilton* [1990, Figure 3], the formation of Eddy B starts in November 1984 (day 1775 in Figure 5a) and ends in July 1985 (day 2032 in Figure 5a). The full cycle has a strong signature in the stick diagram of his current meter G2 at 397 m. However, on the deeper current meters (below 1565 m), the Loop Current signature is mainly visible at the end of the cycle, with rotating currents showing an alternation of northward and southward flows. The same vertical distribution and timing of the deep flow events is observed in the MICOM simulation as shown by Figure 10m.

5.2. Vortex Propagation

[34] The ubiquity of mode one in the instability process of the Loop Current ring is responsible for the generation of a cyclone north of the anticyclone that will survive longer than the other cyclones (Figure 11f). Their interaction with the planetary vorticity gradient will sustain the drift of the dipole to the west as a result of the beta gyre evolution [*Sutyrin and Morel*, 1997]. The vertical signature of the instability explains the generation of the northern cyclone in the deep layer of the vortex, as shown on Figures 10k and 10l. Therefore the β effect provides another explanation, in addition to that of *Cushman-Roisin et al.* [1990], for the generation of the horizontal dipole coined "modon" in the Loop Current ring literature. Comparing Figure 10l with Figure 11f shows an intensification of the cyclone south of the Loop Current ring, trapped between the eastern Yucatan shelf, the western Florida shelf and the Loop Current in port to port regime. This cyclone could be intensified as a result of forcing by the Loop Current.

[35] The above results suggest that the cyclones produced by the instability of the Loop Current ring rim contribute to the separation of the Loop Current ring from the Loop Current by enhancing the westward drift of the ring. The remote control mechanism of the separation process remains the β effect, as first shown by *Hurlburt and Thompson* [1980].

6. Summary and Conclusions

[36] The analysis of the deep circulation in the eastern Gulf of Mexico using the MICOM simulation reveals interesting correlations between the motion in the deep water and the Loop Current regimes. This ECMWF daily forced simulation shows good agreement with the observations in terms of both short-scale and long-term temporal variability, supporting the previous results of *Romanou et al.* [2004].

[37] The net transport in the Yucatan Current is in good agreement with the recent observations of *Sheinbaum et al.*

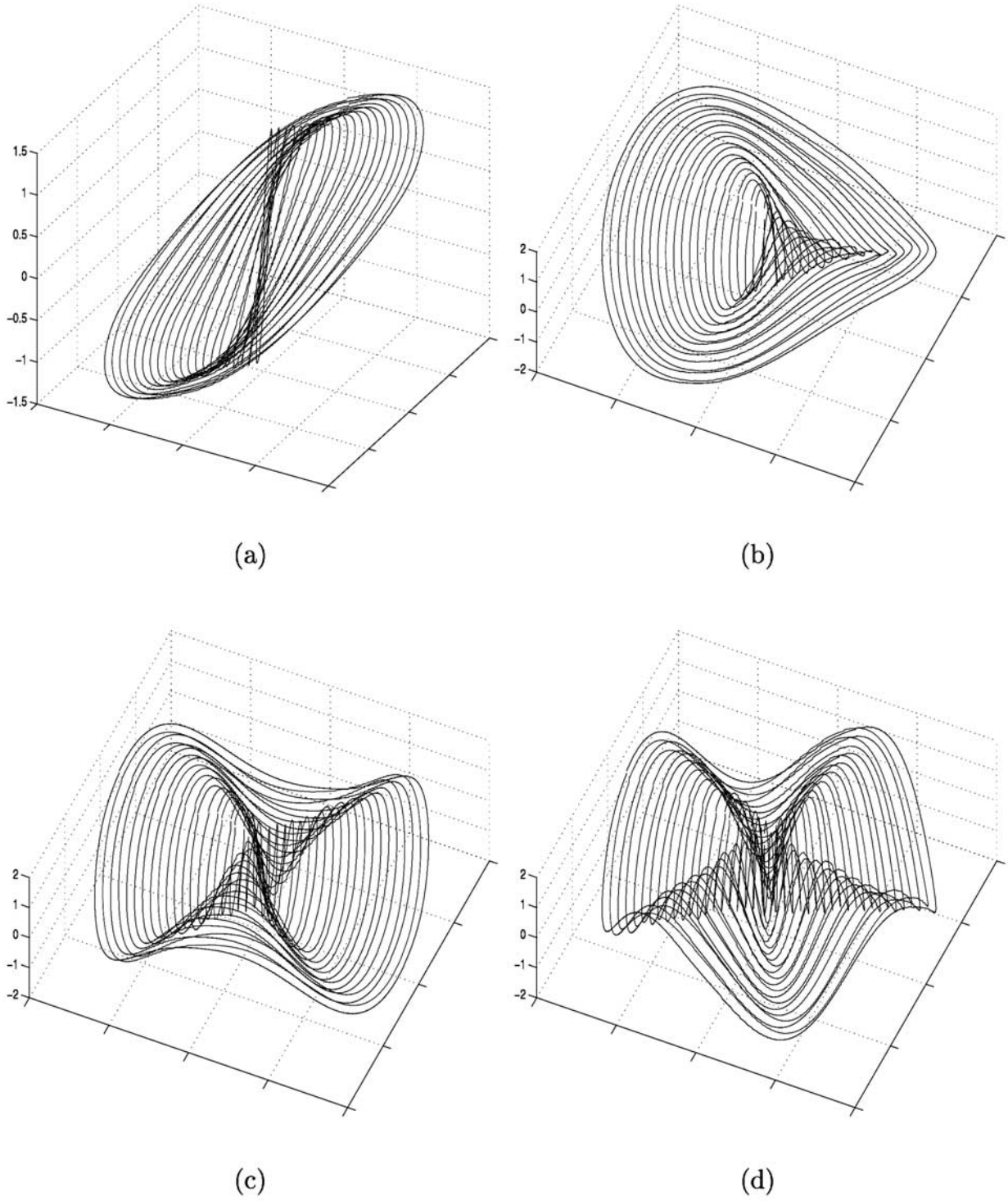

Figure 12. Spatial structure of mode (a) $m = 1$, (b) $m = 2$, (c) $m = 3$, and (d) $m = 4$.

[2002] as well as with historical and modeling estimates. The surface transport is characterized by a tripolar structure in the Yucatan channel: the main inflow into the Gulf of Mexico (i.e., the Yucatan Current) and the outflows along the Cuban and Mexican sides. Indeed, the Loop Current oscillates in longitude, shifting to the center of the channel as the transport increases and moving back to the west when the inflow decreases. The outflow in the deep water, and also on one or both sides of the Yucatan Current, increases its transport as a response to the increase of the Yucatan Current inflow.

[38] The main characteristic periods are 110 and 221 days, and 8.4 months. The first period likely corresponds to the forcing of the Caribbean eddies in the Yucatan Current and is also dominant in the lateral shift of the Loop Current maximum. Therefore the lateral shift of the Loop

Current maximum is also related to the Caribbean eddy forcing. The second period is the double harmonic that was observed by *Maul et al.* [1985] in his deep current measurements in the Yucatan Current. The last period appears to be connected to the ring formation and is identical to the usual ring shedding cycle studied by *Maul et al.* [1985], *Sturges* [1992, 1993], and *Vukovich* [1995]. The lengths of the six cycles studied here are, respectively, 12, 15.2, 19.8, 7.5, 8.5, and 15 months, with an average of 13 months, which is exactly the average length of a cycle found by *Sturges* [1992].

[39] This study also shows the strong correlation between the Loop Current regimes and the deep circulation. The growth of the Loop Current in the model results, or its northward migration, was found to be in good agreement with the theoretical results of *Pichevin and Nof* [1997] and *Nof and Pichevin* [2001]. There is first a ballooning of the Loop Current loop in which its surface area increases, followed by the separation of the ring from the Loop Current under the β or topographic effect. The separation process itself is related to an instability whose signature is the sudden deepening of the Loop Current deepest layer and the spinning in this layer. The dynamical signature extends deeper than 2000 m (Figure 5b). This sudden acceleration and deepening is shown to be the consequence of an instability growth. It means that the length of the cycle depends more on the potential vorticity distribution and on the stratification in the Loop Current vicinity than on the transport itself. The final separation results from one of the remnant cyclones generated by the unstable process, which will couple with the deep anticyclone to form the horizontal dipole observed in all of the previous numerical experiments. This structure moves northwestward guided by the bottom topography, shedding the ring formed by the Loop Current.

[40] **Acknowledgments.** The study is supported by the Mineral Management Service under contracts 1435-01-00-CT-31076 and 01-99-CT-31028 (via SAIC) and by NSF grant OCE 03-271808. The authors thank W. J. Schmitz Jr. and W. E. Johns for fruitful discussions and contributions to this paper. They also thank L. T. Smith for careful reading and editing of the manuscript.

References

Atkinson, L. P., T. Berger, P. Hamilton, E. Waddell, K. Leaman, and T. N. Lee (1995), Current meter observations in the Old Bahama Channel, *J. Geophys. Res.*, *100*, 8555–8560.

Bunge, L., J. Ochoa, A. Badan, J. Candela, and J. Sheinbaum (2002), Deep flows in the Yucatan Channel and their relation to changes in the Loop Current extension, *J. Geophys. Res.*, *107*(C12), 3233, doi:10.1029/2001JC001256.

Candela, J., J. Sheinbaum, J. L. Ochoa, A. Badan, and R. Leben (2002), The potential vorticity flux through the Yucatan Current and the Loop Current in the Gulf of Mexico, *Geophys. Res. Lett.*, *29*(22), 2059, doi:10.1029/2002GL015587.

Carton, J. A., and Y. Chao (1999), Caribbean Sea eddies inferred from TOPEX/POSEIDON altimetry and 1/6° Atlantic Ocean model simulation, *J. Geophys. Res.*, *104*, 7743–7752.

Chassignet, E. P., and Z. D. Garraffo (2001), Viscosity parameterization and the Gulf Stream separation, in *From Stirring to Mixing in a Stratified Ocean*, edited by P. Muller and D. Henderson, pp. 37–41, U. of Hawaii, Honolulu.

Chassignet, E. P., L. T. Smith, R. Bleck, and F. O. Bryan (1996), A model comparison: Numerical simulations of the North and Equatorial Atlantic oceanic circulation in depth and isopycnic coordinates, *J. Phys. Oceanogr.*, *26*, 1849–1867.

Coats, D. A. (1992), The Loop Current, in *The Physical Oceanography of the U.S. Atlantic and Eastern Gulf of Mexico*, edited by J. D. Milliman and E. Imamura, chap. 6, U.S. Dep. of the Interior Min. Manage. Serv. Atl. OCS Reg., Herndon, Va.

Cochrane, J. D. (1972), Separation of an anticyclone and subsequent developments in the Loop Current (1969), in *Contributions on the Physical Oceanography of the Gulf of Mexico*, edited by L. R. A. Capurro and J. L. Reid, pp. 91–106, Gulf Publ. Co., Houston, Tex.

Cushman-Roisin, B., E. P. Chassignet, and B. Tang (1990), Westward motion of mesoscale eddies, *J. Phys. Oceanogr.*, *20*, 758–768.

da Silva, A. M., C. C. Young, and S. Levitus (1994), Atlas of surface marine data 1994, technical report, NOAA, Silver Spring, Md.

Elliott, B. A. (1982), Anticyclonic rings in the Gulf of Mexico, *J. Phys. Oceanogr.*, *12*, 1292–1309.

Ezer, T., L.-Y. Oey, H.-C. Lee, and W. Sturges (2003), The variability of currents in the Yucatan Current: Analysis of results from a numerical ocean model, *J. Geophys. Res.*, *108*(C1), 3012, doi:10.1029/2002JC001509.

Flierl, G. R. (1988), On the instability of geostrophic vortices, *J. Fluid Mech.*, *197*, 349–388.

Fratantoni, D. M., W. E. Johns, T. L. Townsend, and H. E. Hurlburt (2000), Low-latitude circulation and mass transport pathways in a model of the tropical Atlantic Ocean, *J. Phys. Oceanogr.*, *30*, 1944–1966.

Fratantoni, P. S., T. N. Lee, G. P. Podesta, and F. Muller-Karger (1998), The influence of Loop Current perturbations on the formation and evolution of Tortugas eddies in the southern Straits of Florida, *J. Geophys. Res.*, *103*, 24,759–24,779.

Garraffo, Z. D., A. J. Mariano, A. Griffa, C. Veneziani, and E. P. Chassignet (2001), Lagrangian data in a high-resolution numerical simulation of the North Atlantic I, Comparison with in situ drifter data, *J. Mar. Syst.*, *29*, 157–176.

Garraffo, Z. D., W. E. Johns, E. P. Chassignet, and G. J. Goñi (2003), North Brazil Current rings and transport of southern waters in a high resolution numerical simulation of the North Atlantic, in *Interhemispheric Water Exchange in the Atlantic Ocean*, *Elsevier Oceanogr. Ser.*, vol. 68, edited by P. Malanotte-Rizzoli and G. Goñi, pp. 375–409, Elsevier, New York.

Goñi, G. J., and W. E. Johns (2001), A census of North Brazil Current rings observed from TOPEX/POSEIDON altimetry: 1992–1998, *Geophys. Res. Lett.*, *28*, 1–4.

Hamilton, P. (1990), Deep currents in the Gulf of Mexico, *J. Phys. Oceanogr.*, *20*, 1087–1104.

Hoffmann, E. E., and S. J. Worley (1986), An investigation of the circulation of the Gulf of Mexico, *J. Geophys. Res.*, *91*, 14,221–14,236.

Hurlburt, H. E., and J. D. Thompson (1980), A numerical study of loop current intrusion and eddy shedding, *J. Phys. Oceanogr.*, *10*, 1611–1651.

Hurlburt, H. E., and J. D. Thompson (1982), The dynamics of the Loop Current and shed eddies in a numerical model of the Gulf of Mexico, in *Hydrodynamics of Semi-enclosed Seas*, edited by J. C. J. Nihoul, pp. 243–298, Elsevier, New York.

Indest, A. W. (1992), Ring dynamics in the western Gulf of Mexico, Ph.D dissertation, Old Dominion Univ., Norfolk, Va.

Johns, W. E., T. N. Lee, R. Beardsley, J. Candela, and B. Castro (1998), Annual cycle and variability of the North Brazil Current, *J. Phys. Oceanogr.*, *28*, 103–128.

Johns, W. E., T. L. Townsend, D. M. Fratantoni, and W. D. Wilson (2002), On the Atlantic inflow to the Caribbean Sea, *Deep Sea Res.*, *49*, 211–243.

Kay, S. M. (1987), *Modern Spectral Estimation*, Prentice-Hall, Upper Saddle River, N. J.

Larsen, J. C. (1992), Transport and heat flux of the Florida Current at 27°N derived from cross-stream voltages and profiling data: Theory and observations, *Philos. Trans. R. Soc. London, Ser. A.*, *338*, 169–236.

Larsen, J. C., and T. B. Sanford (1985), Florida Current volume transport from voltage measurements, *Science*, *227*, 302–304.

Leaman, K. D., R. L. Molinari, and P. S. Vertes (1987), Structure and variability of the Florida Current at 27°N: April 1982–July 1984, *J. Phys. Oceanogr.*, *17*, 565–583.

Leaman, K. D., P. S. Vertes, L. P. Atkinson, T. N. Lee, P. Hamilton, and E. Waddell (1995), Transport, potential vorticity, and current/temperature structure across Northwest Providence and Santaren Channels and the Florida Current off Cay Sal Bank, *J. Geophys. Res.*, *100*, 8561–8569.

Lee, T. N., F. Schott, and R. Zantopp (1985), Florida Current: Low-frequency variability of the Florida Current as observed with moored current meter station during April 1982–June 1983, *Science*, *227*, 298–301.

Levitus, S. (1982), Climatological atlas of the world ocean, *NOAA Prof. Pap.*, *13*, 173 pp.

Maul, G. A., D. A. Mayer, and S. R. Baig (1985), Comparisons between a continuous 3-year current-meter observation at the sill of the Yucatan

Strait, satellite measurements of Gulf Loop Current area, and regional sea level, *J. Geophys. Res.*, *90*, 9089–9096.

Molinari, R. L., W. D. Wilson, and K. Leaman (1985), Volume and heat transports of the Florida Current: April 1982 through August 1983, *Science*, *227*, 292–294.

Murphy, S. J., H. E. Hurlburt, and J. J. O'Brien (1999), The connectivity of eddy variability in the Caribbean Sea, the Gulf of Mexico, and the Atlantic Ocean, *J. Geophys. Res.*, *104*, 1431–1453.

Niiler, P. P., and W. S. Richardson (1973), Seasonal variability of the Florida Current, *J. Mar. Res.*, *31*, 144–167.

Nof, D., and T. Pichevin (2001), The ballooning of outflows, *J. Phys. Oceanogr.*, *31*, 3045–3058.

Nowlin, W. D., Jr., and H. J. McLellan (1967), A characterization of the Gulf of Mexico waters in winter, *J. Mar. Res.*, *25*, 29–59.

Ochoa, J., J. Sheinbaum, A. Badan, J. Candela, and D. Wilson (2001), Geostrophy via potential vorticity inversion in the Yucatan Channel, *J. Mar. Res.*, *59*, 725–747.

Oey, L.-Y., H.-C. Lee, and W. J. Schmitz Jr. (2003), Effects of winds and Caribbean eddies on the frequency of Loop Current eddy shedding: A numerical model study, *J. Geophys. Res.*, *108*(C10), 3324, doi:10.1029/2002JC001698.

Paiva, A. M., J. T. Hargrove, E. P. Chassignet, and R. Bleck (1999), Turbulent behavior of a fine mesh (1/12°) numerical simulation of the North Atlantic, *J. Mar. Syst.*, *21*, 307–320.

Papadakis, M. P., E. P. Chassignet, and R. W. Hallberg (2003), Numerical simulations of the Mediterranean Sea outflow: Impact of the entrainment parameterization in an isopycnic coordinate ocean model, *Ocean Modell.*, *5*, 325–356.

Pichevin, T., and D. Nof (1997), The momentum imbalance paradox, *Tellus, Ser. A*, *49*, 298–319.

Richardson, W. S., W. J. Schmitz Jr., and P. P. Niiler (1969), The velocity structure of the Florida Current from the Straits of Florida to Cape Fear, *Deep Sea Res.*, *16*, 225–234.

Romanou, A., E. P. Chassignet, and W. Sturges (2004), Gulf of Mexico circulation within a high-resolution numerical simulation of the North Atlantic Ocean, *J. Geophys. Res.*, *109*, C01003, doi:10.1029/2003JC001770.

Schmitz, W. J., Jr. (2001), On the circulation in and around the Gulf of Mexico. Vol. I: A review of the deep water circulation. http//www.cbi.tamucc.edu/gomcirculation/

Schmitz, W. J., Jr., and P. L. Richardson (1968), On the transport of the Florida Current, *Deep Sea Res.*, *15*, 679–693.

Schott, F. A., T. N. Lee, and R. Zantopp (1988), Variability of structure and transport of the Florida Current in the period range of days to seasonal, *J. Phys. Oceanogr.*, *18*, 1209–1230.

Serra, N., S. Sadoux, I. Ambar, and D. Renouard (2002), Observations and laboratory modeling of Meddy generation at Cape St. Vincent, *J. Phys. Oceanogr.*, *32*, 3–25.

Shay, L. K., A. J. Mariano, S. D. Jacob, and E. H. Ryan (1998), Mean and near-inertial ocean current response to Hurricane Gilbert, *J. Phys. Oceanogr.*, *28*, 858–889.

Sheinbaum, J., J. Candela, A. Badan, and J. Ochoa (2002), Flow structure and transport in the Yucatan Channel, *Geophys. Res. Lett.*, *29*(3), 1040, doi:10.1029/2001GL013990.

Sturges, W. (1992), The spectrum of Loop Current variability from gappy data, *J. Phys. Oceanogr.*, *22*, 1245–1256.

Sturges, W., J. C. Evans, S. Welsh, and W. Holland (1993), Separation of warm core rings in the Gulf of Mexico, *J. Phys. Oceanogr.*, *23*, 250–286.

Sutyrin, G. G., and G. R. Flierl (1994), Intense vortex morion on the beta-plane: Development of the beta gyres, *J. Atmos. Sci.*, *51*, 773–790.

Sutyrin, G. G., and Y. G. Morel (1997), Intense vortex motion in a stratified fluid on the beta-plane: An analytical model and its validation, *J. Fluid Mech.*, *336*, 203–220.

Vukovich, F. M. (1995), An updated evaluation of the Loop Current's eddy-shedding frequency, *J. Geophys. Res.*, *100*, 8655–8659.

Welch, P. D. (1967), The use of fast Fourier transform for the estimation of power spectra: A method based on time averaging over short, modified periodograms, *IEEE Trans. Audio Electroacoust.*, *15*, 70–73.

Welsh, S. E., and M. Inoue (2000), Loop Current rings and the deep circulation in the Gulf of Mexico, *J. Geophys. Res.*, *105*, 16,951–16,959.

E. P. Chassignet and L. M. Chérubin, Rosenstiel School of Marine and Atmospheric Science, University of Miami, Miami, FL 33149, USA. (echassignet@rsmas.miami.edu; lcherubin@rsmas.miami.edu)

W. Sturges, Department of Oceanography, Florida State University, Tallahassee, FL 32306, USA. (sturges@ocean.fsu.edu)